Geological Solutions: Pre-Bid Risk Assessment and As-Built Claims in the NY Metropolitan Region

Charles Merguerian[1], Ph.D., P.G. and J. Mickey Merguerian[2], M. Sci.

[1]Duke Geological Laboratory, 55 Spongia Road, Stone Ridge, NY 12484; CharlesM@Dukelabs.com
[2]Dukelabs DSC, Inc., 16 Middle Lane, Westbury, NY 11590; Mickey@DukelabsDSC.com

ABSTRACT

To evaluate pre-bid construction risk and to support successful as-built differing site condition (DSC) claim recoveries over the years, we have applied simple geological techniques to consults throughout the NYC Metropolitan region. Such techniques have documented a broad array of anomalous subsurface geological issues resulting in impeded as-built production rates and expanded costs. These issues were detected in varied geological terrains for both TBM and traditional drill and blast tunnels, subsurface excavations, large-diameter vertical shafts and in caisson- and pile installations. The as-built issues resulted in costly remediation efforts and DSC claims in instances where unanticipated geological anomalies produced short stand-up times, excessive water- and material inflows resulting in job-suspending sidewall- and crown collapse, voids and invert heave in tunnels and unstable shaft walls.

Below, we share some geological techniques that have allowed us to provide support for as-built DSC claims from a number of local construction efforts. All of these cases depended upon proving anomalous as-built conditions compared to normal anticipation by bidding contractors based on provided pre-bid geotechnical information. Based on specific site conditions, these techniques have included: traditional mapping, lithologic- and structural analysis, petrographic analysis, stereonet analysis, rock mass density studies, comparative statistical studies of pre-bid data vs. as-built recovery (REC %), Rock Quality Designations (RQD %) and unconfined compressive stress (UCS) data, controlled subaqueous video mapping efforts resulting in 3-D mapping of shafts and rock sockets, and three-point problem solutions. The analyses have provided lithologic (mineralogy, texture, density and metamorphic grade) and geological data on buried rock masses to better craft subsurface rock removal techniques and to identify and support DSC claims.

Together, such simple geological techniques have proven to be crucial in providing a testable, scientific basis for identifying departures from reasonably anticipated rock mass conditions and to support successful DSC claims for both owners and contractors.

INTRODUCTION

Since 1975 we have been involved in numerous DSC claims for various large-scale subsurface projects in the NYC region including drill and blast and TBM tunnels, large diameter shafts and installation of subaqueous and subsurface caissons and piles for our clients. We have drawn from our expertise in structural geology, petrography, geochronology, geochemistry, geotechnical engineering and statistical analysis to represent both owners and contractors where

we sought to provide a scientific basis for both the denial and award of claims. Although there is no substitute for thorough pre-bid risk assessment, we find that professional geological input is rare in the bidding process because of time restrictions in the bidding process, this despite telephone books worth of geotechnical data for larger projects that is largely glossed over until as-built issues arise. Thus, we tend to become engaged after problems occur and when costly remediation techniques were employed to increase production and mitigate losses.

Although we will not disclose the precise locations of these job sites, we have selected three construction efforts that document our use of basic geological solutions in client support for tunnels, subaqueous bridge shafts and terrestrial drilling of caissons for building excavations.

TBM TUNNEL

Costly by their very nature and occurring in an unforgiving subsurface environment, tunnel drives in hard rock crystalline terrains require careful geotechnical analysis. DSC claims in such efforts are significant in scope and cost. Our work in tunnels spans four decades and from these efforts we choose one to share in this paper. We refer you to four papers concerning geological controls on effective hard rock TBM tunneling in crystalline terrains that delve further into the details and parameters of tunneling in NYC (Merguerian 1994, 2005a, 2005b, 2008).

TUNNEL #1

The first construct we would like to highlight took place in the late 1990s and was a roughly 5-mile-long, 23’2” diameter water tunnel bored by a Robbins hard-rock single beam TBM – the most powerful TBM ever built and utilized at the time (Figure 1).

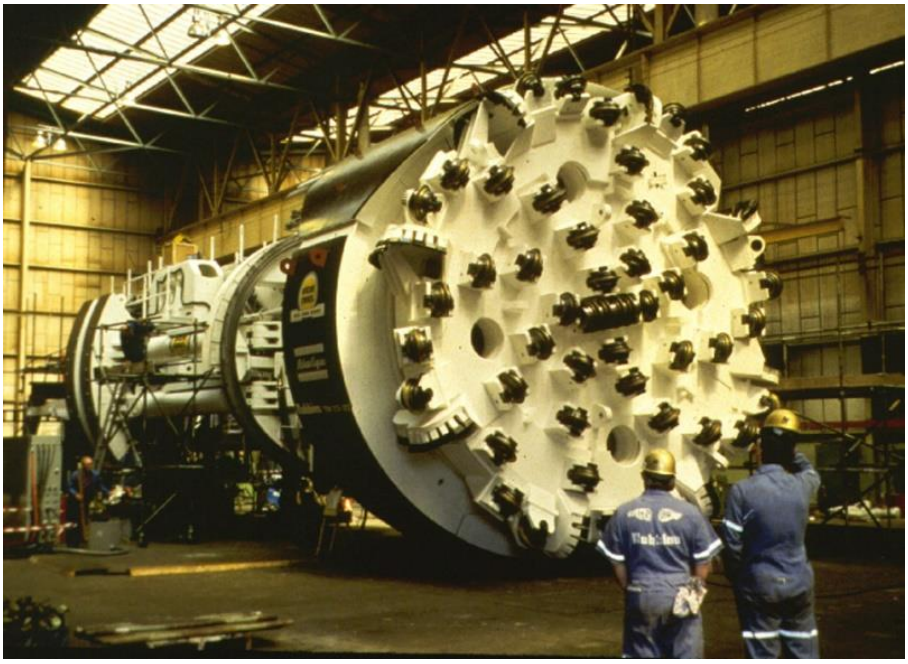

Figure 1 – View of front 84’ of the roughly 300’ long Robbins single-beam hard rock TBM (Model 235-282) which was assembled in the bellout at base of main access shaft of Tunnel #1.

The main issues encountered on this tunnel drive were much lower than anticipated TBM advance rates, sidewall and crown instabilities and short stand-up times, water inflows and invert heave. These resulted in missed construction deadlines and expanded costs. The main culprits in this case were a faulty Geotechnical Baseline Report (GBR), a contract document which identified the wrong NYC rock formation (Hartland Formation) for the alignment. The boring logs contained incorrect lithologic assignments and the pre-bid drilling program was too widely spaced and under-analyzed. Overall rock mass properties were vastly different from contractor anticipation. This consulting engagement required a number of parallel geological efforts rooted in detailed mapping of the entire tunnel, petrographic analysis of collected rock specimens, rock mass statistical analyses on lithotypes, mineralogy and density and geochronologic analysis. Using TBM performance data we were able to show decreased TBM advance rates and utilization in zones of mapped geological anomalies (Merguerian and Ozdemir 2003).

Mapping. Over the three-year period of our engagement on this tunnel project, we mapped 1.75 million ft^2 of tunnel at a scale of 1" = 10' in order to fully document the tunnel walls including ductile geological structure, brittle faults and joints (including orientation, width, filling type and consistency, roughness, seepage, displacement and mineral coatings), areas of bad ground needing additional support, zones of anomalous garnet concentration and anomalous water inflows. Field checking of contacts took place incrementally and measurements were entered into a database for statistical analysis. Over 3,000 digital images, 35 mm Kodachrome slides and videos were keyed by tunnel stationing for documentation and future DSC claim use.

The presence of iron in the service locomotive tracks, metal air and water piping, ductwork, and the conveyor system precluded the use of a magnetic Brunton compass for strike-and-dip measurements. After discussions with our dear friend SC (Geologist, NYC DEP), we constructed a laser-pointer leveling device that was able to accurately measure the strike of features with respect to the surveyed tunnel trend (Figure 2).

Figure 2 – Mechanism used for measuring strike of features exposed on both tunnel walls at springline and comparing to surveyed invert orientation. Dips were measured using Brunton compass and verified by cartographical calculations from map geometries.

By climbing up on the piping of the tunnel wall springline and having a clear view of the other wall springline, planar features such as faults, foliation, and dikes were relatively easy to view and trace across the crown. A bubble level was then used to hold horizontal one ruler section on the feature to be measured and the laser pointer was used to sight the feature on the opposite springline position. The true north angle of strike of any feature was easily calculated with respect to the surveyed invert trend. Great care was taken to properly calibrate the device to the centerline trend in the various curves of the tunnel. By the end of this phase an upgraded mylar-and-ink field map was produced for each 100' section of the tunnel (Figure 3.)

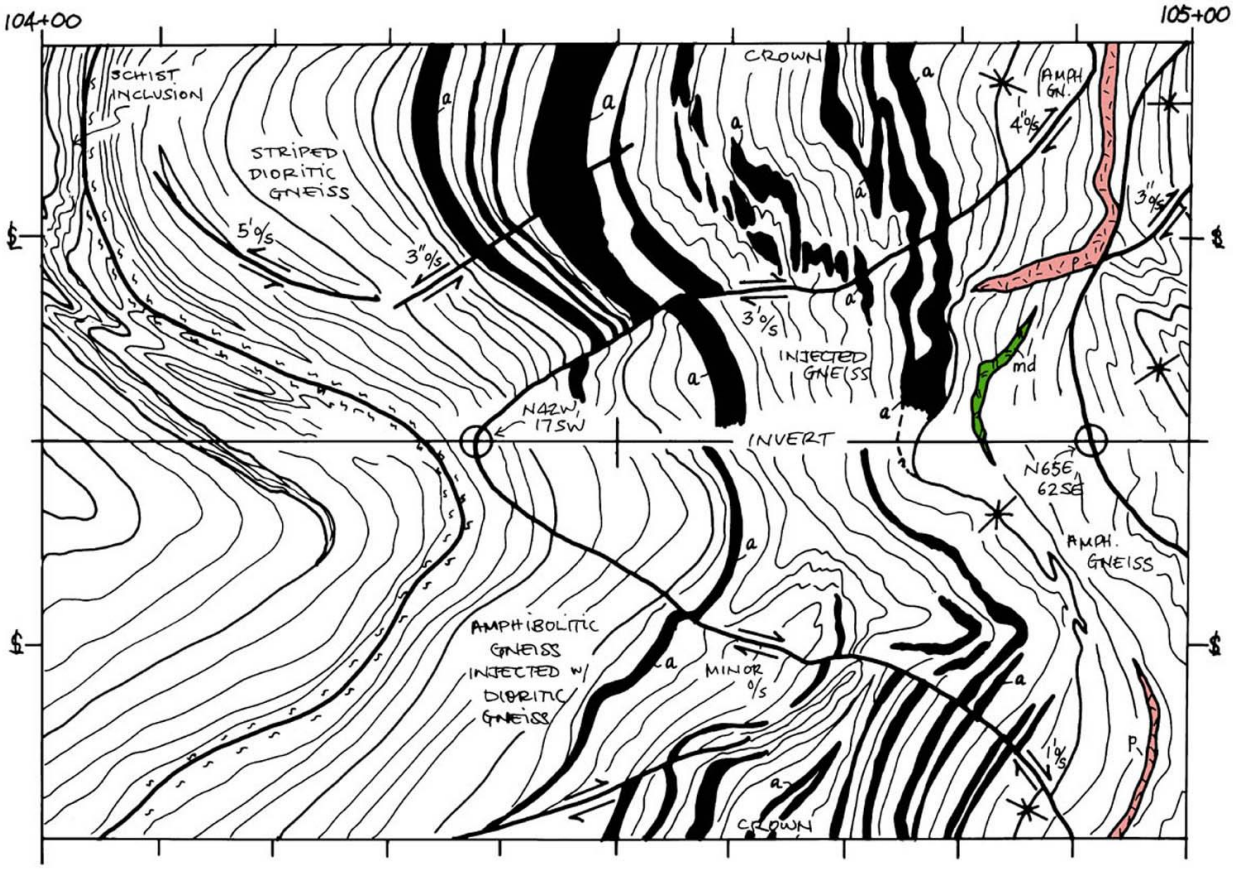

Figure 3 – Geological map of Tunnel #1 shows granulite-facies amphibolite gneiss and younger dioritic orthogneiss cut by pegmatite (p) and a mafic dike (md). The amphibolitic gneiss is locally sheared but clearly occurs as inclusions in the dioritic gneiss. The tunnel invert is shown along the center of the map and the tunnel walls curl upward into a cylinder to join at the crown. The position of the tunnel springline is shown at the map edge. This map, one of 250 in the unpublished Tunnel #1 Map Portfolio, records 100' of the tunnel. Here, a low-angle reverse fault oriented N42°W, 17°SW cuts the invert at Station 104+38 (tunnel invert bearing is N22°E). A younger N65°E, 62°NE brittle fault cuts the invert at Station 104+91. Original map scale 1" = 10'; tunnel diameter 23' 2".

Internal rock fabrics (gneissic layering) and faults were checked using compass oriented rolled mylars of the individual maps utilizing a Brunton compass. Such measurements disclosed

that the gneissic fabric exposed in Tunnel #1 was not in a favorable orientation for efficient TBM mining. Although the pre-bid data indicated a NE-trending moderate to steep SE-dipping rock fabric, stereonet analysis (Figure 4) of the gneissic layering between Stations 4+00 and 254+00 demonstrated that 26 of 235 poles (11%) indicated subhorizontal layering and that 64 poles (27%) show gentle dips (less than 30°). Thus, subhorizontal to gently dipping rock fabrics underlie broad tracts (~38%) of Tunnel #1. This low-angle structural grain of Tunnel #1 presented an unfavorable rock fabric orientation for efficient TBM chip production and contributed to the problem of rock powdering (excessive fines) and low advance rates.

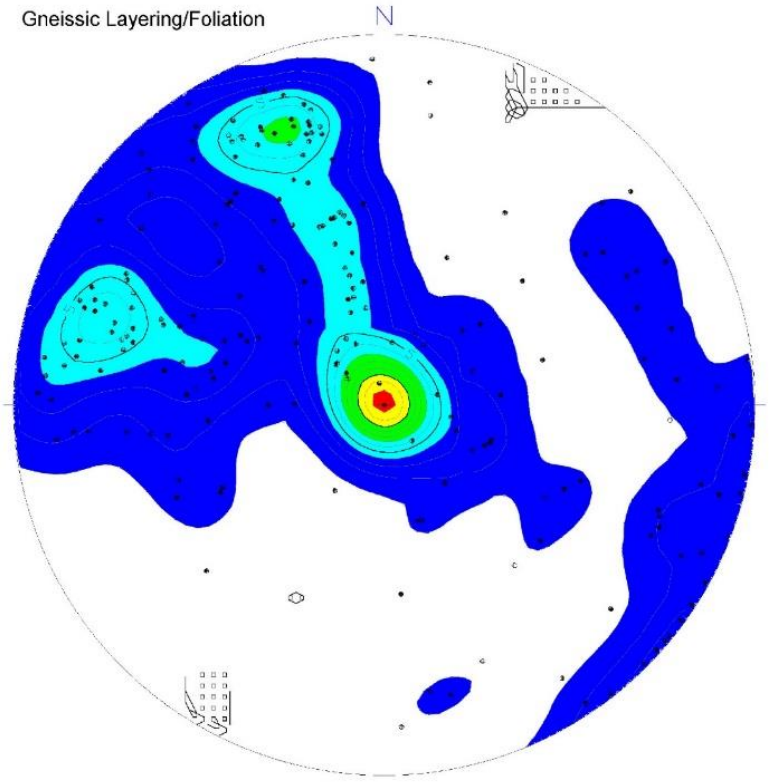

Figure 4 – Gently inclined clustering of stereonet poles (~38%) together with anticipated NNE- and ENE-strike and moderate to steep scattered SE dips of gneissic layering/foliation (n = 254).

Petrographic Analysis. Petrography, one of the best tools used in geological analysis of rocks, allows for microscopic examination crystal textures and identification of minerals. The process involves collection of rock samples or use of rock core and precise preparation of petrographic slides which are 30-micron thick slices of rock sandwiched between two pieces of glass (base slide and a thinner cover slip) which together form a rock "sandwich" held together by epoxy of known optical index. Petrography, in conjunction with geological mapping, revealed that the structural and metamorphic history of rocks of Tunnel #1 were <u>not</u> Paleozoic Hartland Formation. Compare the rock textures shown below in Figure 5 between foliated rocks of typical Hartland Formation (Figure 5A) with those found in Tunnel #1 (Figure 5B) exhibiting granoblastic textures. Proper petrographic analysis would have alerted bidders to this departure from pre-bid anticipation but sadly, little petrographic work was conducted on this job.

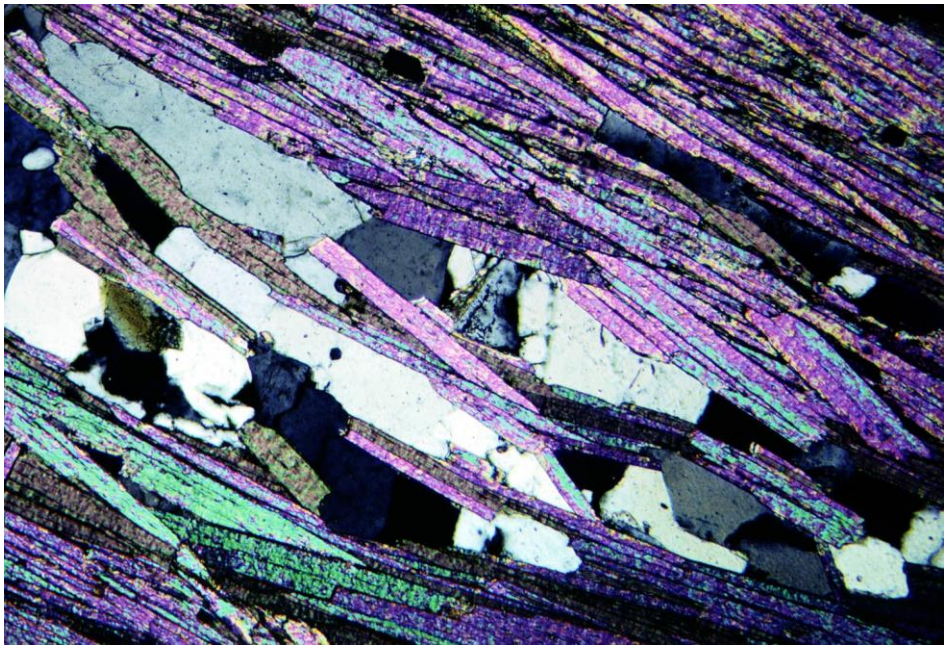

Figure 5A – Photomicrograph in crossed nicols of aluminous Hartland schist (Sample N403-1; World Financial Center site, lower Manhattan). The section shows fine-textured lenticular quartz and minor plagioclase (white and gray) separated by aligned muscovite and minor biotite (highly colored crystals). Such directional mineral growth results in a penetrative micaceous foliation that splits readily under stress because of the parallelism of relatively soft mica flakes.

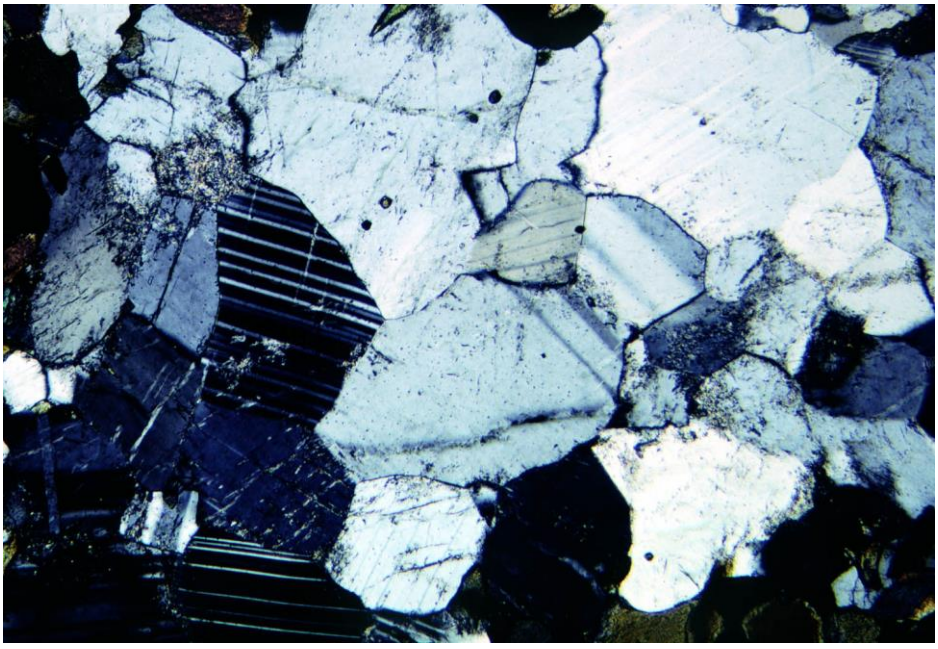

Figure 5B – Photomicrograph in crossed nicols of Tunnel #1 leucocratic gneiss (Sample Q085; Station 159+80) showing granoblastic intergrowth of plagioclase and minor quartz. Note the granular texture, the stable 120° crystal boundaries of the interlocking plagioclase and interstitial quartz and the lack of any penetrative foliation. Both photomicrographs are 2 mm across.

Alignment Borings. Typical core logs include information on fracture density, recovery, lithology, and sometimes the nature of fracture surfaces. Statistical studies on the borings should include recording detailed lithologic, mineralogic, and petrographic characteristics by a trained professional geologist. Integrated research on the actual core should be targeted at the depth of the tunnel horizon but comparative analysis outside the tunnel horizon will better identify rock mass trends and identify possible changes that could result in detrimental surprises during tunneling. All of the core should be examined by the same geologist to establish consistency and core logging by drillers without professional certification in geology or geological engineering should not be relied upon without careful rechecking. In particular, anomalous lithologies are the common cause of changed condition losses in underground work. Professional geologists are more likely to accurately identify anomalous lithologies – many examples of misidentified rock types have resulted in tunneling inefficiencies related to changed conditions.

A comparison between mapped Tunnel #1 lithotypes vs. those depicted in the borings logs at the tunnel horizon showed that the logs did not identify the proportion of various rock types (Figure 6). This resulted in an improper choice of TBM cutterhead tooling (cutter metallurgy, number and diameter) for the planned tunnel drive.

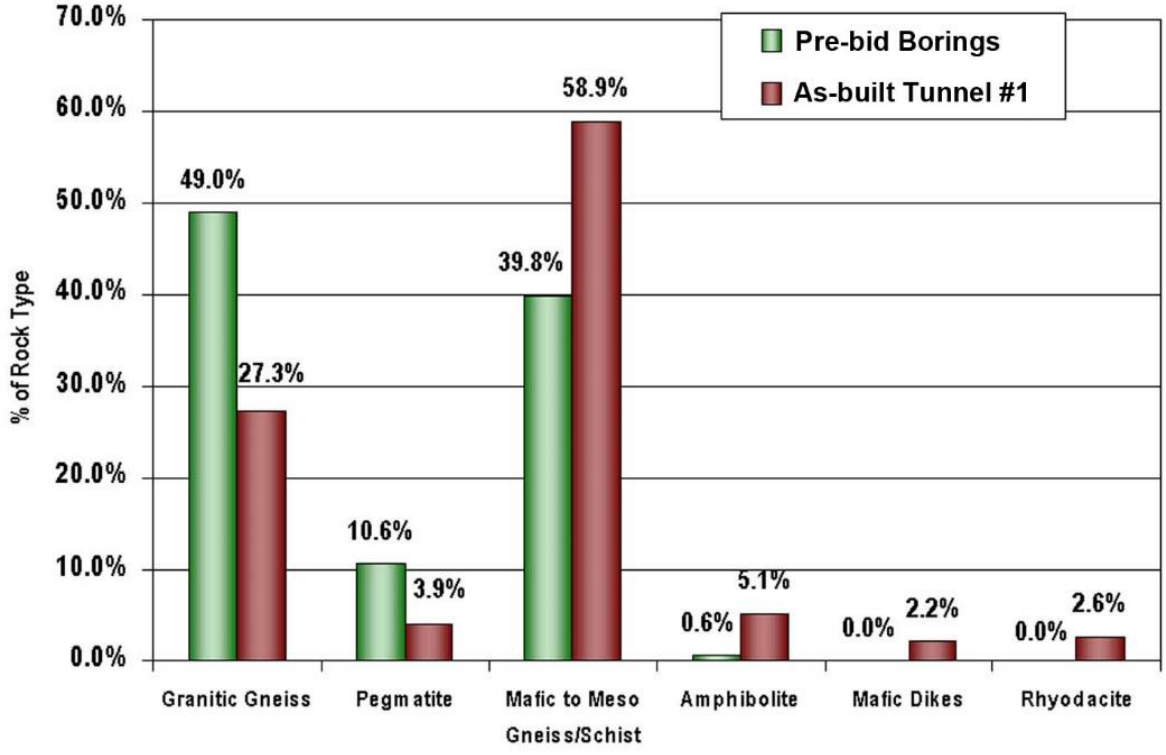

Figure 6 - Bar graph showing disparity between anticipated lithotypes identified by examining pre-bid borings (green) vs. those found to occur in the tunnel drive based on as-built mapping (red). Note the difference in the relative proportion of granitic and pegmatitic (felsic) rocks vs. the mafic, amphibolitic, and mesocratic (mafic and intermediate) rocks and the presence of unanticipated rocks of rhyodacite affinity. This lithologic variation from pre-bid anticipation proved an impediment to efficient mining. (Adapted from Merguerian and Ozdemir, 2003.)

Density Analysis. A simple measurement often overlooked, the density or specific gravity of rocks is a simple and useful litmus test for predicting TBM or drilling penetration rates. Higher density rocks are less penetrable simply because they tend to contain dense/hard minerals such as garnet, pyroxene, and aluminosilicate minerals sillimanite and kyanite. Density is readily measured using simple, inexpensive apparatus (Merguerian 2005a). A density profile along the tunnel alignment can help understand this variation over a planned TBM drive and can help identify anomalous trends or anticipate zones of unusual rock mass properties (Figure 7).

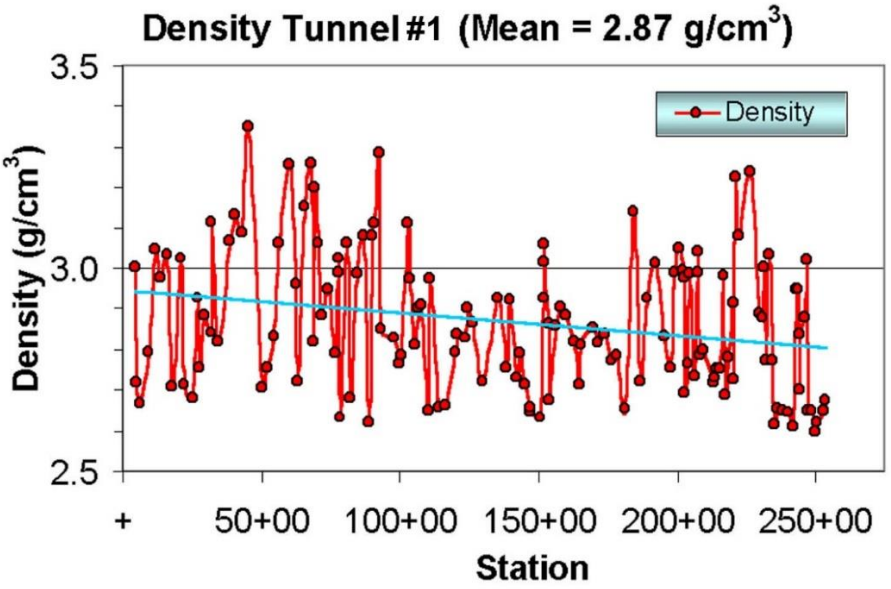

Figure 7 – Rock mass density variation as compiled from sawn slabs from 161 samples collected during as-built mapping of Tunnel #1, NYC. The graph indicates that the bulk density of the tunnel varied from 2.62 to 3.35 gm/cm^3 and that density decreased slightly toward the higher stations (sloping blue line) as shown by the mapping. The mean density (2.87 g/cm^3) was in keeping with the lithotype analysis that indicated that more intermediate- to mafic lithologies by comparison to what the pre-bid borings indicated. (See Figure 6.) Typical schistose and interlayered granofels such as anticipated in the Hartland Formation should have averaged about 2.55 g/cm^3. (Adapted from Merguerian and Ozdemir 2003.)

Penetration Rates. Average TBM penetration rates of <2 m/hour were encountered in Tunnel #1 during excavation rather than the 3m/hour anticipated. Despite the fact that pre-bid documents provided by the owner indicated that the Hartland Formation was anticipated along the tunnel alignment, as-built structural, lithologic, and petrographic studies showed that the rocks of Tunnel #1 consisted of tough orthogneiss of mesocratic, mafic and leucocratic composition. These metaigneous rocks developed coarse-textured fabrics during Grenvillian high-pressure granulite facies metamorphism, and retained their nearly anhydrous, poorly foliated character during subsequent high-grade Ordovician and younger deformation and upper amphibolite facies metamorphism (Figure 8). Lacking a penetrative foliation, the coarse-textured granoblastic rock texture and extraordinary garnet content of up to 50% in some zones and mapped to underlie ~11% of the entire tunnel (Figures 9A, B; Table 1) together proved an

impediment to efficient chip production and resulted in bimodal production of excessive fines and large blocks that choked TBM grizzlies and damaged conveyor belt systems.

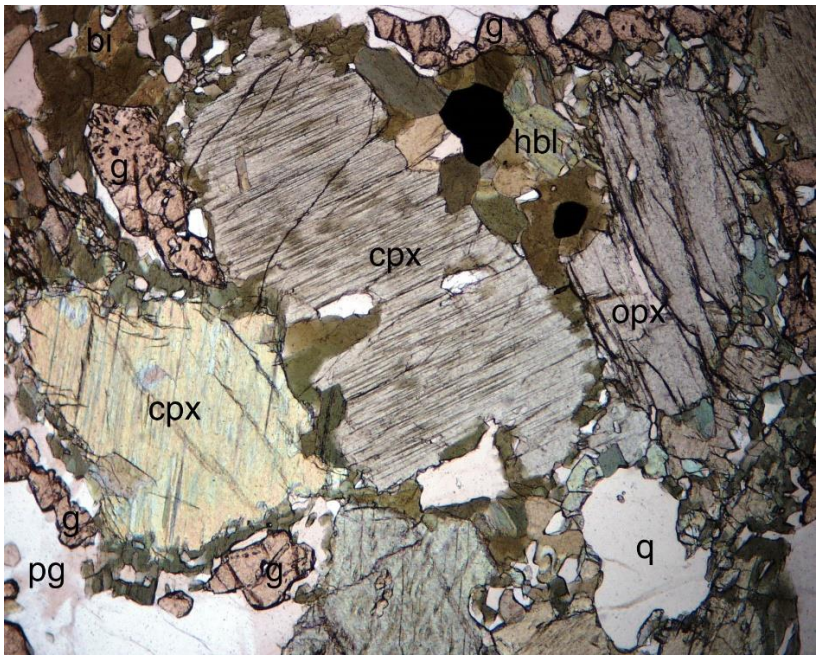

Figure 8 – Photomicrograph in plane-polarized light of Tunnel #1 mafic gneiss showing coarse-textured granulite facies texture in the form of partly recrystallized orthopyroxene (opx), clinopyroxene (cpx), and primary garnet (g). Quartz = q. Note the secondary thin overgrowths of green hornblende (hbl), granular garnet (g) and biotite (bi), the result of late retrograde metamorphic recrystallization. (Sample Q114; Station 15+90; 2 mm field of view.)

A. **B.**

Figures 9A, B – Tunnel views of two of the 32 garnet zones mapped showing the anomalously high concentration (up to 50%) of dense garnet that defines such zones. Highlighted in yellow on Table 1 (below) the garnet zones 9 (Figure 9A.) and 21 (Figure 9B.) were produced during two phases of granulite- followed by upper-amphibolite facies metamorphism as detected during petrographic analysis of mineralogy and rock mass textures.

Table 1 – Compilation of anomalous garnetiferous zones of Tunnel #1 showing that excessive garnet concentrations underlie almost 11% of the tunnel which resulted in untimely TBM cutter wear and the production of excessive fines. Petrographic analysis indicated that garnet production was the result of both primary and secondary metamorphism of the granulite facies metamorphism that effected the terrain. Yellow highlighted zones (Nos. 9, 21) are shown above in Figures 9A and 9B.

Anomalous Garnet Concentrations, Layers, Lenses, and Laminae					
Tunnel #1					
Tunnel Station		**Length**	**Garnet**	**Field Description**	**Samples (Q-)**
Start	**End**	**(Feet)**	**Zone No.**		
27+45	27+80	35	**1**	Garnet layer a few feet thick in migmatitic mafic gneiss, LW only	120
36+18	37+70	152	**2**	Garnet layers and laminae in injected mafic gneiss	
45+00	46+48	148	**3**	Garnetiferous mafic schist, gneiss and amphibolite	128
53+87	54+80	93	**4**	Two garnetiferous layers a few feet thick in mafic gneiss	131A, B
68+03	68+50	47	**5**	Garnetiferous zone in mafic gneiss, RW only	137, 138
68+78	69+84	106	**6**	Garnetiferous mafic schist, gneiss and amphibolite	139
70+27	70+78	51	**7**	10' thick garnet layer in mafic gneiss, schist, and amphibolite	140
71+01	71+18	17	**8**	Thin garnet lenses in mafic orthogneiss	
77+75	79+10	135	**9**	Broad zone of garnetiferous layers, lenses, and laminae	08, 144, 145
95+82	96+22	40	**10**	Garnetiferous leucosome in mafic gneiss, LW only	
96+77	99+25	248	**11**	Broad zone of garnetiferous mafic gneiss, schist, and amphibolite	153
100+13	102+46	233	**12**	Broad zone of garnetiferous mafic gneiss, schist, and amphibolite	155
103+43	103+62	19	**13**	Laminated garnet zone in mafic gneiss, schist, and amphibolite	
104+95	105+43	48	**14**	Laminated garnet zone in mafic gneiss, schist, and amphibolite	158
106+50	108+70	220	**15**	Broad zone of garnetiferous mafic gneiss, schist, and amphibolite	11
109+30	109+35	5	**16**	Blocks of garnetiferous gneissic rock in shear zone	
111+35	111+45	10	**17**	Laminated garnetiferous zone in mafic gneiss, LW only	
123+55	123+70	15	**18**	Laminated garnetiferous zone in mafic gneiss	101
151+80	152+20	40	**19**	Garnetiferous biotite schist and gneiss in contact with dacite	89A, B; 90A, B
171+15	173+78	263	**20**	Broad zone of highly garnetiferous migmatitic mafic rocks	80A, B
175+53	176+45	92	**21**	Broad zone of highly garnetiferous migmatitic mafic rocks	78
180+75	181+48	73	**22**	Garnet lenses and laminae in mafic schist, gneiss, and amphibolite	76
183+10	183+57	47	**23**	Garnet layer and laminae in mafic schist, gneiss, and amphibolite	
183+98	184+57	59	**24**	Garnet layer in mafic schist, gneiss, and amphibolite	75A, B
198+26	198+35	9	**25**	Sheared and rotated block containing garnet layers, RW only	
199+94	201+00	106	**26**	Garnetiferous layers in sheared mafic gneiss	68
201+80	202+05	25	**27**	Garnetiferous layer in mafic gneiss, RW only	14
207+18	207+95	77	**28**	Zone of garnet with layers, lenses, and laminae in mafic gneiss	20, 21
221+12	221+95	83	**29**	Thin garnet layers in mafic gneiss, schist, and amphibolite	33A, B
225+07	225+38	31	**30**	Garnetiferous granitoid at mafic gneiss/orthogneiss contact	
229+72	229+97	25	**31**	Garnetiferous zone in mafic gneiss and schist	
231+25	232+36	111	**32**	Laminated garnetiferous zone in mafic gneiss	38A, B
TOTAL ====>		**2663**	**Linear Feet of Tunnel #1 with Highly Garnetiferous Rocks = (2663/25035) = 10.64%**		

The term garnetiferous appears on nearly every page of the pre-bid boring logs but no percentages are given. Most petrologists would use the term garnetiferous for rocks with a trace to 3% volume %. At higher percentages, the occurrence of garnet is indeed of scientific interest. Yet, no consensus exists on the quantitative use of the term garnetiferous. Clearly the effect of

garnet on production would vary in "garnetiferous areas" depending upon volume percent of the hard, dense mineral. In our view, the entire tunnel is garnetiferous (3% garnet or less) and we regard this as a reasonable baseline. Yet, some areas of Tunnel #1 are so enriched in garnet (30%-50%) that broad use of the term garnetiferous is quite misleading. Such garnet contents would be termed an *"ore deposit"* in many parts of the world.

During TBM mining the importance of garnet hinges on the extreme hardness and high density of the mineral (Hardness 6.5 to 7.5 on Mohs' scale; Density 3.1 to 4.3 g/cm^3). Along with quartz at hardness 7 on Mohs' scale, in concert they produce unusually hard, abrasive rocks when found in high concentration. (See Figures 9A, B and Table 1.) The garnet is commonly found along with quartz (another abrasive mineral) and can occur as finely disseminated garnet, garnetiferous layers a few feet thick, as lenticular lenses, and in highly laminated areas forming broad zones up to 263' long in the tunnel. Garnet is also found in high concentrations within amphibole-pyroxene bearing rocks as garnet+plagioclase segregations. In thin section, thin zones of garnet rim areas of relict orthopyroxene+clinopyroxene the product of secondary metamorphism. (See Figure 8.) Petrographic analysis of Tunnel #1 gneisses demonstrated that high-pressure granulite facies metamorphism promoted the growth of garnet and other dense mineral phases including orthopyroxene and clinopyroxene (Brock, Brock and Merguerian 2001; Spear 1993). Note that high-pressure granulite facies metamorphism is simply not recognized in Hartland Formation rocks in this area of NYC.

TUNNEL #1 SUMMARY

The as-built Tunnel #1 horizon exposes rocks that are clearly <u>not</u> the foliated Paleozoic Hartland Formation of metasedimentary and metavolcanic parentage. Rather, they are Grenvillian migmatitic orthogneiss correlative with the parts of the Proterozoic Fordham Gneiss. During high-pressure granulite facies metamorphism former plutonic igneous rocks transformed into dense, coarse- to medium-textured orthogneiss (metaplutonic rocks) consisting of interlocking crystals of plagioclase, clino- and orthopyroxene, and primary garnet. The microscope showed that a penetrative primary foliation did not develop in the rocks because the deep-seated metamorphic conditions precluded the growth of hydrous foliation-producing phases mica and amphibole. Rather, a granoblastic texture developed which consisted of interlocking plagioclase and intergrown anhydrous mafic minerals. (See Figures 5B and 8.) A second phase of regional metamorphism produced domainal fabrics with localized growth of amphiboles, biotite, and "new" garnet but the "older" granulite textures survived.

Extensive rock testing and TBM performance evaluation studies have provided a correlation between machine performance and natural variations in rock mass properties. The reduced TBM penetration encountered in the construction of Tunnel #1 was caused by higher than anticipated density and rock strength, adverse direction of rock layering and higher rock toughness brought about a high degree of recrystallization and crystal interlocking, the results of their high-pressure granulite facies metamorphic history.

As a result of their metamorphism the rocks developed zones of unusually pronounced garnet content (at least two growth periods identified). The petrographic analysis also showed that the entire tunnel was garnetiferous with unusual garnet concentrations coupled with a high

degree of recrystallization. This created a dense and abrasive rock mass, also confirmed from Cerchar abrasivity measurements. The gneissic rock mass penetrated in Tunnel #1 possessed lithologic properties (texture, anhydrous mineralogy, lithology, density, homogeneity, lack of penetrative mica foliation, and abundant gently dipping fabric orientations) that collectively inhibited efficient TBM mining. In addition, blocky ground conditions resulted in side-wall and crown instabilities from intersecting fault sets (Merguerian 2002, 2015) and from cooling system fracture patterns unique to a suite of glassy, rhyodacite dikes hitherto unknown in the NYC area (Merguerian 2001).

The lessons learned from the Tunnel #1 experience include the recognition that a proper Baseline Geotechnical Report can minimize the pre-bid risks in any subsurface construction effort. In addition to identifying risk in the pre-bid stage, as-built investigations by geologists can define the rock mass conditions and mitigate risks in response to changed conditions.

SUBAQUEOUS BRIDGE SHAFTS

Moving away from crystalline rocks of the Manhattan Prong, the second investigation we would like to share concerns a site in the Newark Basin of New Jersey (Figure 10). This consult involved difficulty in drilling 96" shafts within a gently inclined sedimentary rock unit that underlies a bridge pier site constructed across a river environment. Ironically, we first heard about this consult in 2013 during a coffee break during an ASCE meeting in NYC where we learned that high-water inflows, overnight infilling of casings to base level and infalling blocks of rock plagued the effort and that aquatic life (an eel) was detected in one of the shafts. Abiding by the environmental principle promoted by our dear friend the late Dr. John E. Sanders that *"the fish never lose in court"*, we were interested in the consult and ultimately engaged.

Figure 10 - Physiographic diagram showing the eight major geological provinces in southern New York, northern New Jersey and adjoining states of PA, CT and MA. (From Bennington and Merguerian 2007.)

BOULDERS AND HIGH-WATER INFLOWS

During construction of the bridge, 46 shafts of 96” diameter were drilled using identical means and methods for bridge piers and finished with 90” rock sockets but difficulties in construction were encountered at eight of the shafts on the west side of the river. In these instances, shaft construction was hindered by sink holes, blow-ins, high-water inflows and in-falling blocks of red-colored siltstone and sandstone. The ground conditions required remediation including grouting, additional drilling, reseating of casings and deepening of shafts. A view of the equipment used for subaqueous drilling is shown below (Figure 11).

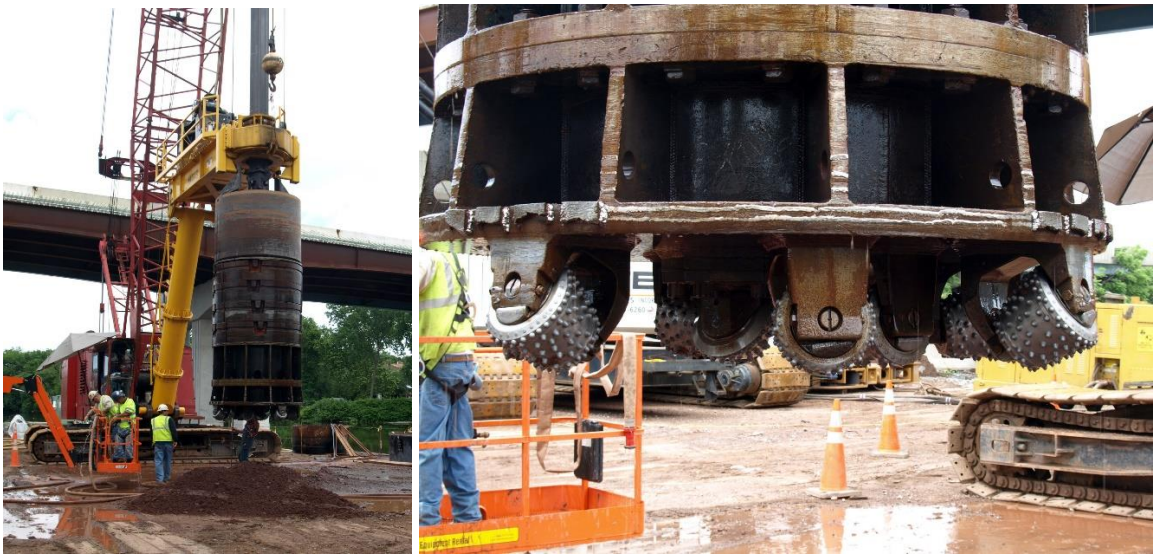

Figure 11 – Westward view of Shaft #23 construction rig near Pier 3 of the job site in New Jersey (L) and close-up view of the cutterhead and cutters (R). (Dukelabs digital images taken 14 June 2013.)

The boulders retrieved from within Shaft #23 examined on-site were sub-angular in shape and somewhat tabular, partially smoothed and consisted of Mesozoic Passaic Formation sandstone and siltstone (Figure 12). Notably, although somewhat similar in appearance to glacial boulders, they exhibited curved scratches indicating circular transport and not the straight parallel striae associated with glacial action. In addition, the boulders did not show the characteristic sub-rounded to rounded shape nor polish glacial boulders and were not exotic but consisted of rock types that are indigenous to the Passaic Formation which underlies the site. One boulder showed parallel joint surfaces outlined with greenish-white mineralization (chlorite+quartz infilling) suggesting the presence of ancient subsurface fractures (joints and/or faults).

Based on the presence of mineralized joints, sub-angular/tabular shape aspect, and curved scratches, our conclusion was that the boulders were locally harvested (not glacial), introduced from the shaft walls during drilling of fractured ground and dragged about during the drilling or mucking process before they were removed from the base of the shaft. Boulder composition was an identical match with the local Passaic bedrock. They were not Paleozoic quartzite or

limestone which had been reported as boulders from within the Passaic Formation by other field workers. These observations forced the conclusion that the boulders were introduced from the shaft walls during construction drilling.

Figure 12 – View of subangular boulders and cobbles of Passaic Formation siltstone and sandstone muck collected from base of Shaft #23. Note the tabular aspect of the boulders, a relic of original bedding, and the incipient polishing by mechanical means. Hammer is 38 cm (15") in length. (Dukelabs digital image taken 14 June 2013.)

High water inflows and blow-ins were also experienced during the drilling. Such inflows could only indicate sub-casing lip hydrologic connectivity to the adjacent river. The presence of intersecting open joints and/or faults are the typical explanations for such phenomenon in this type of shallow subsurface construction setting. Our video surveys and mapping verified this interpretation as discussed below.

We were retained by the contractor to review drilling difficulties and slowdowns during 2010 -2012 for shafts at the bridge site where sidewall instabilities (including within-shaft and rock socket blocky fallout) and excessive inflows of water and sediment. In all, eight (8) out of 45 drilled shafts (17.8%) experienced a similar DSC. A site map of the three western bridge piers (Piers 1, 2 and 3) affected by such issues is shown below as Figure 13.

BEDROCK STRATIGRAPHY AND LITHOLOGY

As we do for most consults, a full review of the geological literature yielded pertinent information. The bridge project site lies within the Mesozoic Newark Basin (See Figure 10.)

which is a vast geological terrain consisting of strata known as the Newark Supergroup, a thick sequence of red-colored sedimentary rocks and four intervening sheets of blackish mafic igneous rock known as the Watchung basalt flows and the Palisades intrusive sheet.

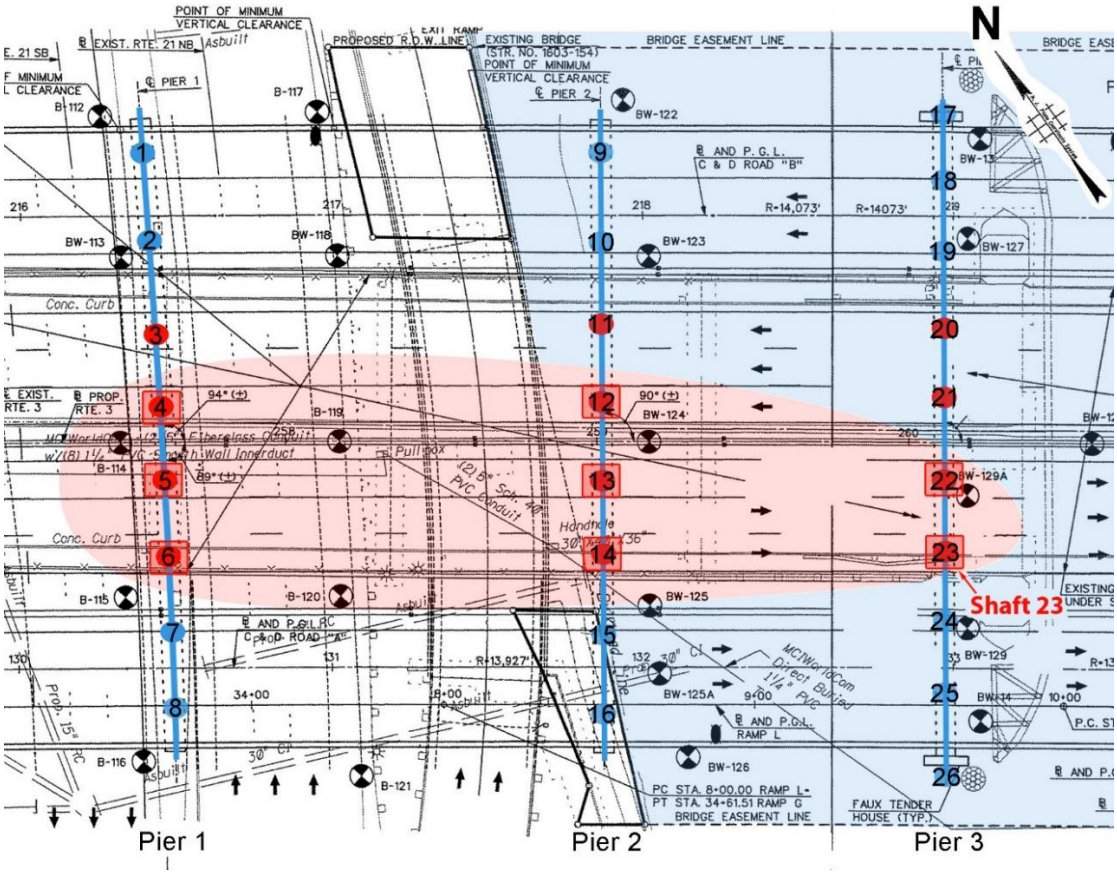

Figure 13 – Site map showing the eight problem shafts (4, 5, 6, 12, 13, 14, 22 and 23 – boxed and numbered red circles) drilled in Piers 1, 2 and 3 and how they define a NW- to SE-trending zone of similar ground effects (pink ellipse) both on land (uncolored) and within the river (blue).

Geological maps show that the rock unit that underlies the job site is the Passaic Formation which consists of a thick (3,550 m) gently NW-tilted sedimentary rock sequence of interlayered red-colored siltstone, shale, and sandstone of Mesozoic age with some stratigraphic horizons, particularly near the Ramapo basin-marginal fault, that contain well-rounded boulders and cobbles of much older Paleozoic rocks (typically quartzite and carbonate) derived from block uplift and erosion of the adjacent Hudson Highlands terrain.

All published references studied describe the Passaic Formation as intact and exhibiting many types of primary and secondary sedimentary structures. Absolutely none of the published research, from over 200 years of study, reported any field or drill-core based evidence of large openings, voids, caves, or caverns within the rock formation which is understandable considering the degree of lithification and lack of readily soluble mineral phases that constitute the Passaic rock mass.

Based on pre-bid boring log driller's notes the predominant rock types (82% or 74 of the 90 runs) were identified as consisting of "fresh" and "medium hard" sandstone of red, brown, red-brown color with minor gray and blue scattered layers. Interlayered "fresh" and "hard" shales of similar coloration account for 18% (16 of the 90 runs). Thus, sandstone predominates over shale in the borings at about a 4.5:1 ratio.

Careful study of the boring data (including a careful statistical analysis of REC % and RQD %, UCS data and geotechnical descriptions indicate that drillers should have anticipated a non-fractured, “medium hard” rock mass of "fair" quality. Based on these and other data, the geotechnical report recommended drilled shafts with sockets for pier and caisson construction and anticipated no highly fractured or faulted ground conditions that would require different means and methods than those recommended and employed by the contractor - yet the eel made its way into the bottom of the shaft!

DISCOVERY OF THE GEOLOGICAL CAUSE FOR A DSC

In order to decipher the as-built contractor experience, we devised and supervised video recordings of a water-filled 96” problem shaft and a developed a down-hole method of mapping the interior of the 90" (7.5') diameter rock socket extending below top of rock in order to generate an associated 2-D map and construct an analog 3-D view of the as-built subsurface geological structure. To calibrate and map the shaft interior we marked the walls by suspending weighted colored ropes with magnetic N, E, S, and W and intervening magnetic compass directions NE, SE, SW, NW clearly visible so that calibration, recording and calculating the orientation of the fractures could be facilitated (Figure 14).

Figure 14 – Various ropes used with weights and C-clamps to hold ropes taught and vertical down the sides of the shaft in order to video each compass rose direction. Analysis of the color-coded videos allowed us to generate an accurate flat 2-D map of the interior of the rock socket.

Careful study of the video was fruitful and allowed for incremental drafting of an accurate 2-D geological map without vertical exaggeration of the 90" (7.5’) Shaft #23 rock socket (Figure 15).

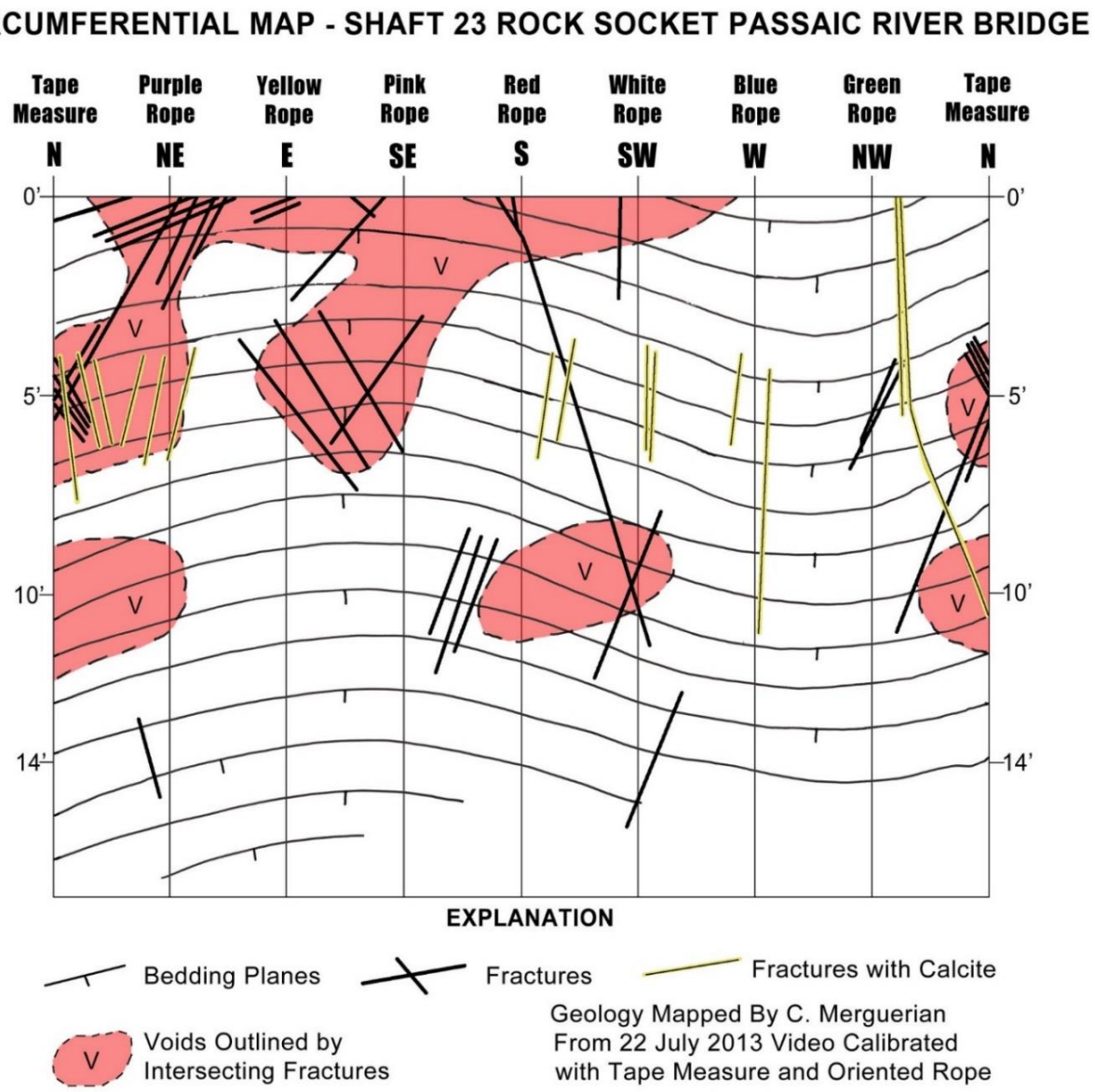

Figure 15 – Circumferential 2-D geological map of bridge Shaft #23 rock socket of 90" (7.5') diameter showing orientation of inclined bedding planes (thin black lines with tick marks), intersecting steep to gentle fractures (thick black lines) and open voids where blocks fell out of socket sidewall (v - pink areas). Also shown are mineralized fractures in yellow and black. Drawn with no vertical exaggeration. Compass directions are magnetic.

The compass-aligned ropes and depth markings allowed for calculation of fracture orientation using standard aligned compass and three-point methods. It was not until the map was printed onto clear acetate and curled by analog methods into a 3-D cylinder to mimic the ~15' deep rock socket did we recognize the alignment of seemingly separate through-going discontinuities (dark black lines in Figures 15 and 16) and the relationship of the fracture intersections to the mapped voids (pink areas in Figures 15 and 16).

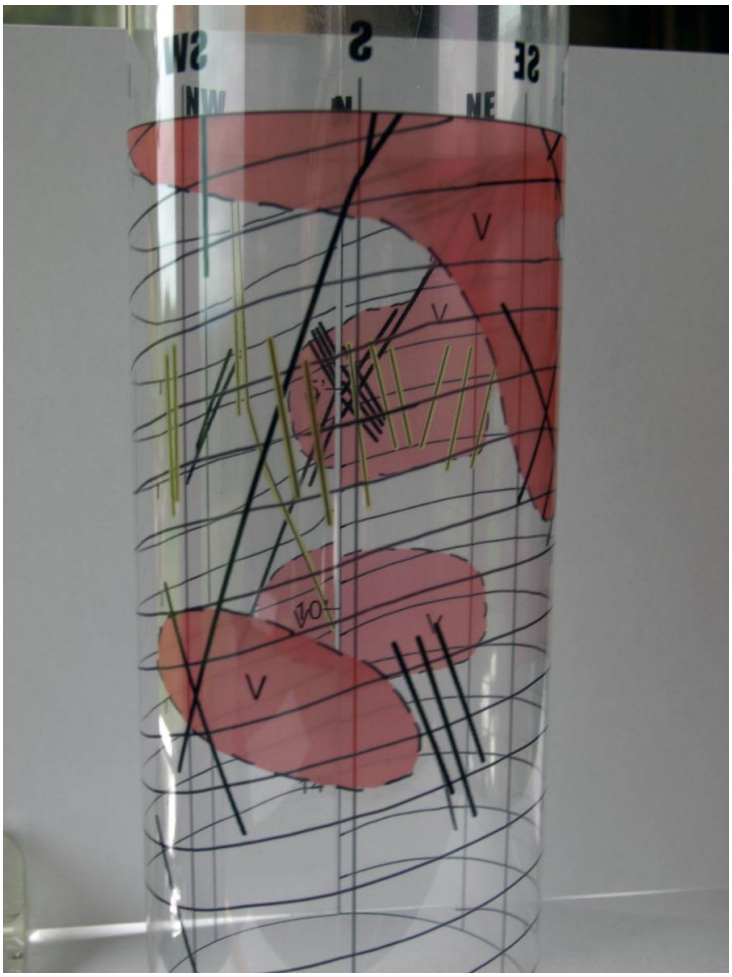

Figure 16 – Northward view of Shaft #23 rock socket acetate map of Figure 15 curled into a cylinder showing the relationship of bedding planes (~14° NW dip [thin closely spaced lines]), NNE-, NE- and NW-trending fractures (steep, black lines), and voids (pinkish areas - v). Note that some of the steeper, NNE-trending fractures (outlined in yellow) are mineralized by calcite or whitish zeolite, common minerals found within faults and joints in the Newarkian strata and also observed in the boulders shown in Figure 12, above. Not obvious are gently inclined (~14°) fractures that parallel bedding near the top of the map at the base of casing.

Figures 15 and 16 show gentle NW-dipping bedding (~14° - thin, closely spaced black lines) and bedding-plane joints near the top of rock cut by high-angle (60°-90°), oft-times mineralized fractures (steep thicker black lines). The steep fractures fall into three major geometric classes. The most prominent and through-going feature is a fissure that extends through the rock socket center and downward over 10' in extent with a N35°E strike and 75°NW dip (center of image in Figure 16). Also mapped were at least five (5) less extensive fractures that parallel this main fissure as is common in fault zones. A second prominent set of fractures strike N40°W and dip 70° toward the NE. There is also a younger, third set of shorter, closely spaced mineralized conjugate fractures with a N25°E strike and 80°SE dip fanning through vertical to dips of 80°NW. These discontinuities overlap and seem to crosscut the older NE-and

NW-trending fracture sets. The steeper conjugate fractures sometimes show mineralization with calcite or a whitish zeolite mineral as indicated by yellow and black markings in Figures 15 and 16. A fourth set of fractures occur near the top of rock. These are closely spaced, shallow in dip and parallel bedding. These are simple bedding plane joints that trend NE and dip very gently (~14°) NW.

Figure 15 shows that four major open voids exist in the drilled rock socket of Shaft #23 from the base of the casing to about 8’ depth, then again at about 10' depth. The voids are 3’ to 8’ in extent, extend a few feet deep into the sidewall and are concentrated up-dip in the eastern half-perimeter of the rock socket as would be expected if the blocks initially slid along bedding-parallel fracture planes into the rock socket. Many of the open voids were found to terminate against steep planar fractures surfaces suggesting emphatic fault control. Figures 15 and 16 clearly document the relationship between areas of multiply fractured bedrock and associated voids.

The site inspections, video analysis and mapping performed indicated that open voids and blocky ground conditions experienced at the bridge site by the contractor during rock socket drilling were the result of amplification of geological effects produced by the convergence of four sets of natural geological discontinuities (faults and joints). Unfortunately for this bridge construction effort, the gently inclined bedding plane joints intersected by multiple generations of steep to vertical fractures (joints and probable faults) together created blocky ground and difficult construction conditions using standard means and methods. All of these related effects (unstable shaft- and socket walls with in-falling blocks of rock and sidewall water- and material-inflows) greatly impeded construction. The pre-bid geotechnical information provided to the bidders did not inform the contractors of such conditions as no mention of faults much less intersecting faults were noted. The unanticipated ground behavior at the eight bridge pier shafts during drilling constituted a DSC as no one could have reasonably anticipated the effects of such localized highly fractured ground from the provided pre-bid information and other available data.

Note that on Figures 13 and 17 that the eight DSC caissons (Shafts #4, 5, 6, 12, 13, 14, 22 and 23) are not evenly distributed throughout the jobsite but are spatially oriented with a NW to SE alignment parallel to the NW-SE faults. This is additional evidence for a DSC with 17.8% of the 45 shafts affected as the extension of mapped faults conforms to the pink ellipse of affected shafts shown in Figure 17. Thus, there appears to be geological explanation of cause and effect.

Multiple fault and fracture convergence as found at the Shaft #23 site are unusual geometric subsurface conditions. Convergent high-angle fractures superimposed on gently inclined bedding plane joints created blocky ground and the excavation led to voids because of fallout from the sidewalls. The Shaft #23 site showed changed site conditions but the projection of fracture trends to other shaft sites explained the formidable extent of bad ground conditions extending out from the Shaft #23 zone of fracture convergence and intersection.

SUBAQEOUS BRIDGE SHAFTS SUMMARY

The investigation of rock conditions in scientific support of a DSC claim in connection with this subaqueous bridge shaft drilling program included site inspections, geotechnical report

analysis and map-based geological analysis. This investigation documented open voids and unstable sidewall conditions at Shaft #23 and provided a natural geological cause for the DSC. Anomalies at Shaft #23 extended northwestward to include other shaft sites where similar voids and blocky, unstable ground with exceedingly short stand-up times resulted in excessive water- and material-inflows and shaft sidewall blocky fallout suggesting far-ranging fault effects of the N40°W-trending fault set that dips ~70°NE. (Compare Figures 15 through 17.)

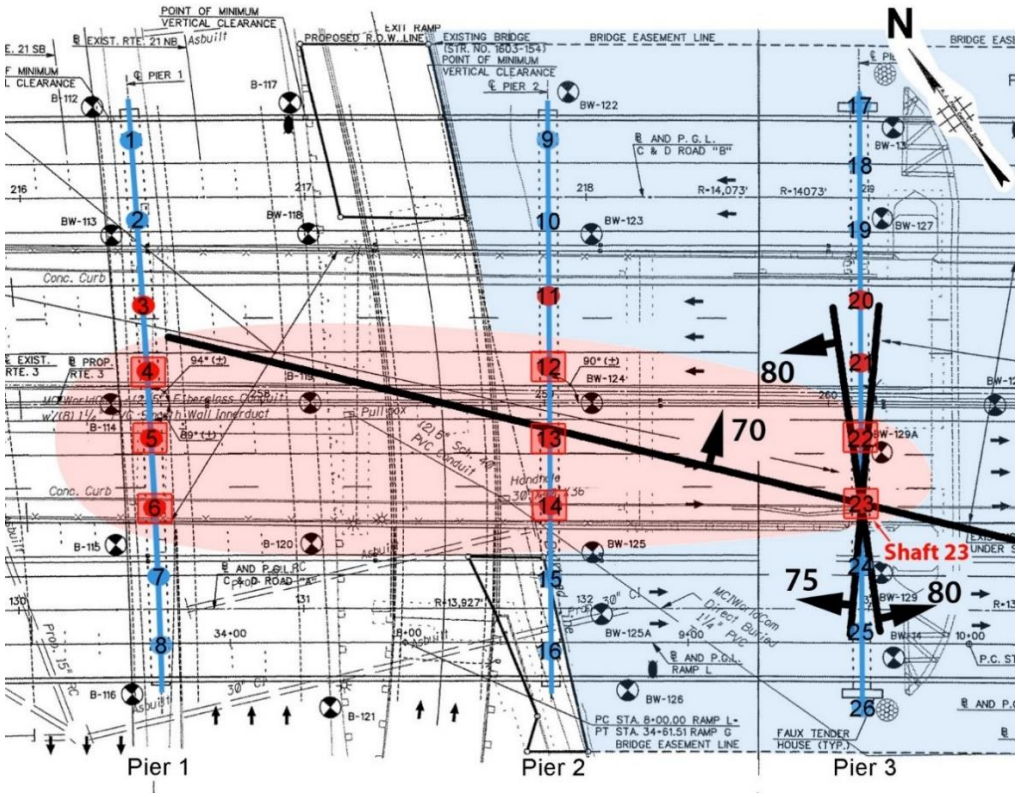

Figure 17 – Plan view of DSC claim area (pink ellipse) that includes the eight problem shafts encountered during Piers 1, 2 and 3 drilling of the bridge. The faults and related joints mapped and shown in Figures 15 and 16 from Shaft #23 are plotted to show their crosscutting relationships and structural control on the associated problem shafts of the DSC claim. Note the three steep fracture systems (N40°W strike, 70°NE dip; N35°E strike, 75°NW dip and N25°E strike with conjugate dips fanning from 80°NW through vertical to 80°SW). These intersecting fractures extend outward from that zone of convergent intersection and cut gently inclined in-situ bedding planes and sub-parallel shallow joints at Shaft #23. Note that all faults were plotted with respect to True North as the magnetic declination at the site in 2013 was -12° 50' (12° 50'W of True North).

These hitherto unknown natural subsurface geological conditions impeded construction using industry standard means and methods and were the basis for successful DSC claims by an experienced contractor as no one could have reasonably anticipated such rock mass conditions (convergent faults at Shaft #23) from the documents provided pre-bid nor from the existing scientific literature.

TERRESTRIAL CAISSONS/PILES

The third geotechnical vignette we share here involves unanticipated ground conditions encountered during down-the-hole hammer drilling for installation of multiple caissons and piles for a high-load above-ground construct in the Manhattan Prong of NYC. This site occurs above nearly 100' of Holocene fill and Pleistocene glacial strata which bury gently inclined lower Paleozoic rocks of the Inwood Marble Formation. Production drilling for forty-four (44) or ~30% of 148 caissons installed experienced anomalous groundwater and/or sediment inflows and associated ground effects during construction, well beyond any reasonable anticipation of risk. Penetration both at the base of the overburden and while drilling rock sockets produced enormous outpourings of water + material including spectacular instances of geysering transforming this NYC construction site into a *"Disney water theme park"* (Figure 18). Below we discuss the ground effects experienced during production drilling using an approved down-the hole hammer and our use of a three-point fracture plane solutions, geological maps and sections to depict the natural bedrock condition detected beneath the site that led to a DSC claim.

Figure 18 – View of as-built anomalous water + material flow and geysering associated with ~100' deep caisson drilling in November 2015 at the job site. (Contractor image.)

The DSC claim pursued by the contractors was based on unanticipated high transmissivity and communication at the base of the overburden and within the upper part of the marble bedrock layer which introduced water and material into many caissons and rock sockets. After costly excessive water debacles on site in 2015 through 2016 we were able to examine the soil and rock core samples in early 2017 to aid our geotechnical analysis.

The scientific conclusions of our geotechnical support efforts rely partly on a basic three-point solution analysis of like features noted in the pre-bid boring logs and our prior experience elsewhere in the same formation. Here we detected through-going, gently-inclined open water-bearing fracture zones dipping beneath the job site that produced an unknown subsurface *"plumbing system"* which fed the excessive water and sediment flows encountered during subsurface drilling. Extraction and redistribution of subsurface water and sediment not only hindered the construction effort but created deleterious ground effects (anomalous extraction flow volumes, ground cracks, cratering, boils and local building settlement and cracking) which led to periods of site demobilization. The two hitherto unknown natural water-bearing transmissive fracture zones identified in this analysis clearly constitute a DSC that no contractor could have predicted particularly in view of the pre-bid geotechnical information provided.

The stratigraphy of roughly 100’ of overburden from the top down include Holocene fill, Pleistocene sand units, intervening varved strata and basal till below (Figure 19). Penetration into the Inwood Marble bedrock were met with persistent excessive water and material outflows that in a few cases led to uncontrollable 40'-high geysering consisting of groundwater and sediment at the drill site. (See Figure 18.)

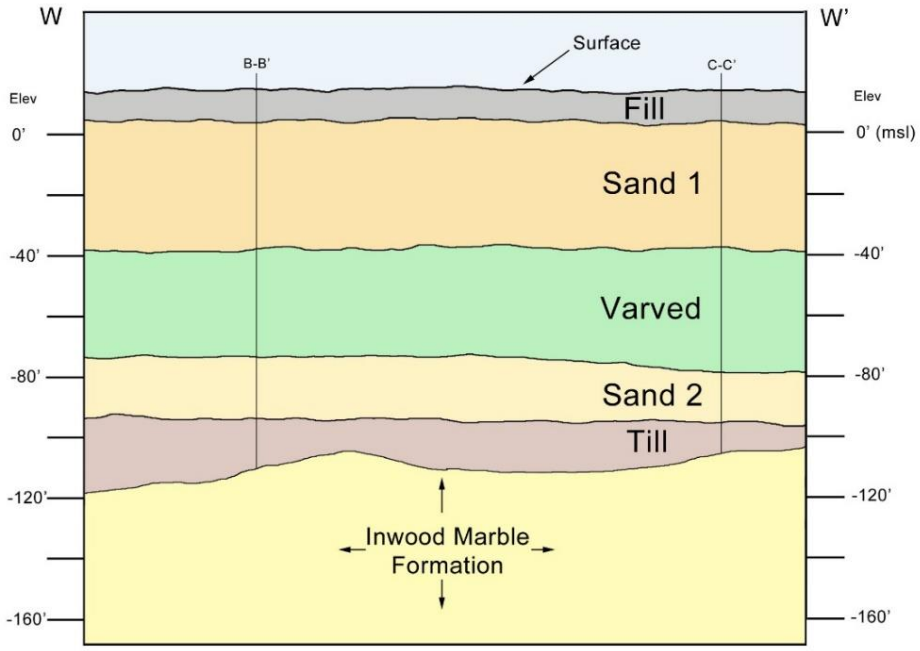

Figure 19 – Across site roughly W-E geological profile section drawn from data supplied in the geotechnical report showing overburden strata and the buried Inwood Marble bedrock layer. This view of the site was the anticipation and design criteria for the contractor’s approved means and methods. (Drawn without vertical exaggeration.)

The problem caisson sites were <u>not</u> scattered throughout the site footprint which argued against any notion of improper means and methods (down-the-hole hammer systems) which were approved by the owners. Rather, the problem caissons were clustered in the northeastern corner of the site (Figure 20) near an adjacent, unsupported old-construction brick and mortar building which settled, tilted, cracked and became severely damaged. What is more, water and material communication occurred between widely separated drilled caisson/pile sites indicating significant subsurface connectivity of transmissive features. Site reports by the contractors and the owner's resident engineers reported *"heavy water, sand, and rock; excessive water from casing; thick (heavy) sediment inflows up to 25'; seams; rock ledges; dirty discharge; large rocks; sockets making water; communication between open drill sites; flooding of the jobsite; spoils on the ground; and equipment damage including broken shoes, rig tilting, hammer clogging and unanticipated hammer firing."*

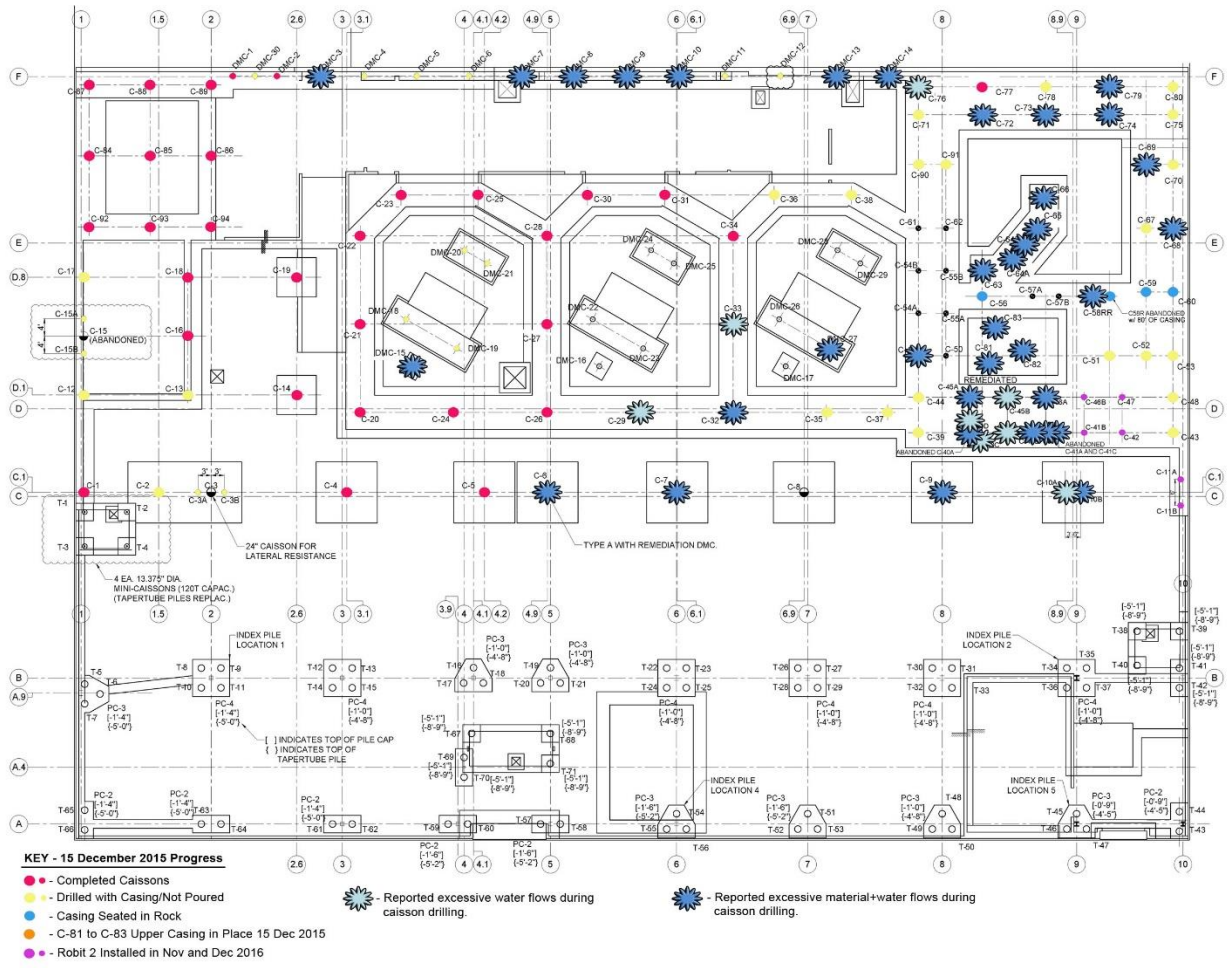

Figure 20 – Site plan showing the clustering of forty-four (44) caisson sites where installation was met with construction difficulties associated with flowing water only (light blue symbols) and water + material outflows (dark blue symbols). The remaining caisson sites shown in red, yellow, orange, black, noncolored and purple were drilled without difficulty. Project north to top of map.

BORINGS AND BORING LOG ANALYSIS

In order to better understand the pre-bid anticipation vs. the as-built contractor experience, we performed a careful study of the geotechnical information provided by two geotechnical reports and 17 associated boring logs. Figure 21 shows the positions of the 17 pre-bid borings performed in 2007 and 2013 and whose logs were included with the geotechnical reports. These data were used by contractors to evaluate the subsurface conditions and formulate baseline parameters for their winning bid and the means and methods for the construction project. Little data on foliation or compositional layering was to be found in the boring logs but the orientation of foliation joints show gentle dips (0° to 30°) for many of these primary features.

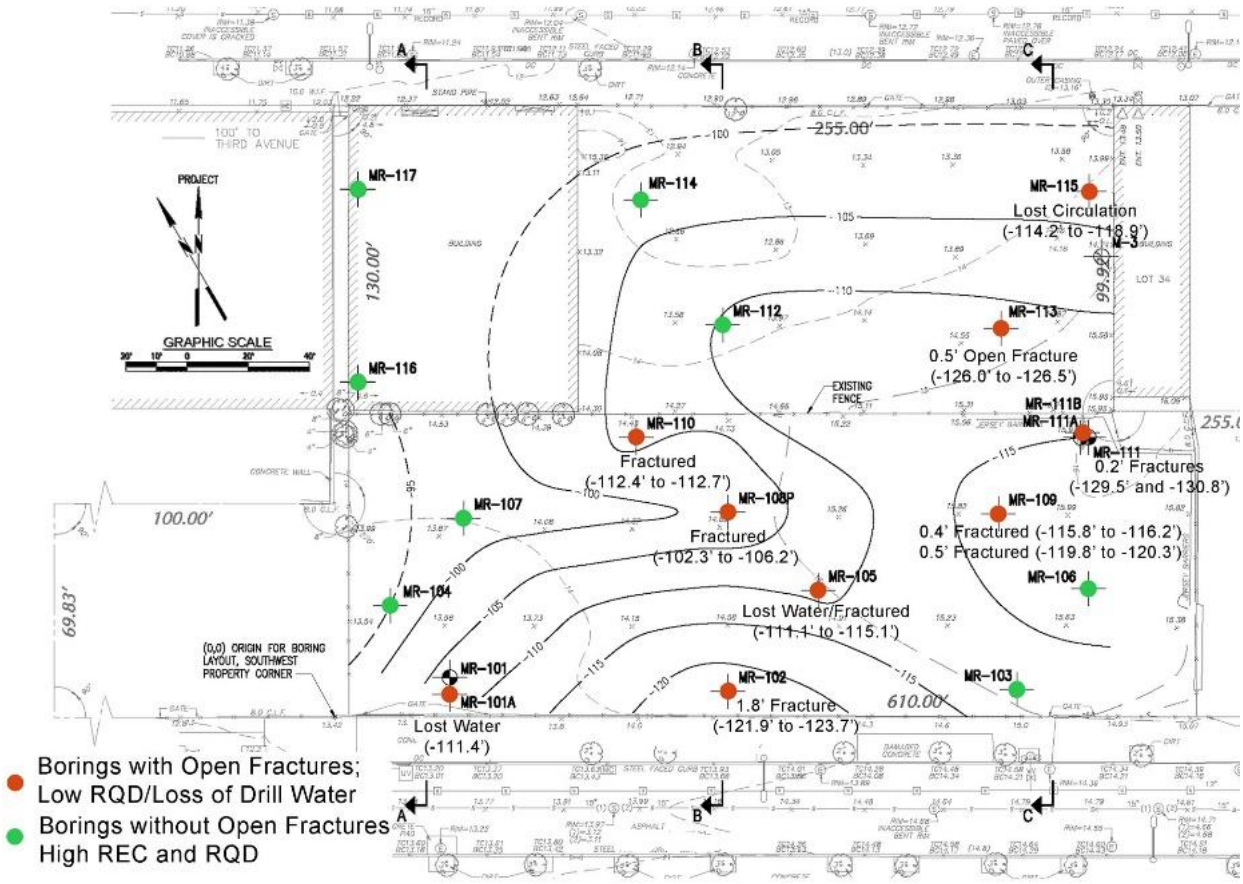

Figure 21 – Site plan map showing topographic data, annotated boring locations (MR-series) and top of rock contours within the footprint of the site. Nine borings with open fractures, low recovery and RQD values, and/or reported *"loss of drill water"* are shown in red. Eight competent borings without reported open fractures and with high recovery and RQD values are shown in green. Note the roughly E-W clustered trend of the red borings.

Examining the soil and core samples in February 2017 confirmed that no contractor could have anticipated the true ground conditions. Visual inspection showed that the core was competent and tended to be massive with some jointing. Thus, a pre-bid core analysis by any

contractor bidding for work and guided by the supplied information on REC and RQD % would create an anticipation of hard- to medium-hard, blocky to closely jointed marble but would provide no hint as to the lateral extent, connectivity, nor potential for hydrologic transmissivity of any fractures within the marble rock mass.

Rather, the as-built experience involved cross-hole communication, excessive water inflows, sediment flows, ground settling, ground cracks and cratering at caisson sites, indicating hidden difficulties within the rock mass. Our as-built analysis indicated that the subsurface fracturing is not sporadic but defined at least one and probably two gently inclined open-aperture fractures that varied from thin seams to fracture zones possibly up to 4.7' thick both near and below the top of rock. Both fractures intercept the top of rock, are separated by about 10' of competant rock and dip about 1° (upper fracture) and 5° (lower fracture) eastward beneath the site. Careful study of inspection videos showed the open fractures despite their blurry subaqueous murky setting, yet the owner and their representatives would not accept our results and a lengthy mediation battle took place that was just recently settled by mediation in 2021.

THREE-POINT FRACTURE PLANE SOLUTIONS

Once boring logs were converted from depths to elevations comparable features detected in the logs allowed us to group borings showing similar traits. This allowed for application of a simple tried and true mining visualization technique (the three-point problem solution) to identify strike and dip of a planar feature given three points of varying depth and known geographic position. The technique assumes uniformity of strike and dip and planarity of the feature which are reasonable assumptions given the small footprint of the site – about a half a NYC block. The technique is a graphical/trigonometric one that involves identification of a maximum, minimum and intermediate elevation of a planar feature such as a mineralized ore vein or through-going fault or fracture (Donn and Shimer 1958). By drawing a triangle that encloses the surface position of sets of three boreholes, as depicted in Figures 22 through 25, a unique point on the line that joins the maximum and minimum elevation values can be scaled that equals the intermediate elevation. A drawn line joining this scaled point to the intermediate boring shows, by definition, a line of equal elevation (strike or trend) of the planar feature. Calculation of dip is straightforward once the strike and the variation of high and low pierce points are identified using standard fold-line techniques.

To solve for dip using orthographic projection, a fold-line is drawn perpendicular to the strike line which then marks the trace of the vertical plane containing the dip section. By rotating this vertical plane 90° upward into the plan view about the fold line one can project the minimum and maximum points parallel to the strike line away from the triangular map to intercept the fold line (map trace of the dip section). By projecting the maximum and minimum penetration points onto the dip section and plotting the change in elevation the dip angle can be measured with a protractor and verified by trigonometric calculation.

The clues that drew our attention came in the form of three widely separated borings that reported *"loss of drill water"* (MR-101A, MR-105, and MR-115). Loss of drill water below top of rock is usually an indication of open voids or fractures. MR-101A lost drill water at -111.4' elev., MR-105 lost drill water between -111.1' and 115.1' elev. (a 4.0' interval), and MR-115 lost

drill water between -114.2' and -118.9' elev. (a 4.7' interval). Since no casing was used in driving NX-core, drill water can escape the borehole at the initial pierce point of a void or fracture despite the report of lost drill water over a 4.0' (MR-105) to 4.7' (MR-115) interval. As such, these values can be considered maximum width values for these features. Alternatively, the void or fracture may encompass the entire interval. In order to perform the three-point analysis, we employed an average *"loss of drill water"* elevation value for MR-105 (-113.1' elev. in Figures 22, 23 and 24) and MR-115 (-116.6' elev. in Figures 22 and 24).

Using the method described above, Figure 22 (three-point problem solution #1) shows that three *"loss of drill water"* borings provided a solution that identifies an open fracture or fracture zone oriented N37°W, 1.5°NE. In order to test for and verify the lateral extent of the feature detected in Figure 22 we also grouped boring MR-101A, MR-105, and MR-115 as similar because of an RQD drop in Run 3C (64%) after much higher values in Runs 1C, 2C and 4C (REC and RQD % values both ranged from 95%-100% in these runs) and the logging of open (0.3') fractures. This allowed for two additional three-point solutions (Figure 23 and 24) which yielded nearly identical strike and dip solutions. (Compare Figures 22 through 24.)

Figure 23 (three-point problem solution #2) shows an open fracture oriented N12°E, 1°SE for borings MR-101A, MR-105, and MR-110. Figure 24 (three-point problem solution #3) shows an open fracture oriented N3°W, 1.5°NE for borings MR-105, MR-110, and MR-115. Keeping in mind that strike varies greatly for very gently inclined features and is, in fact, infinite as one approaches 0° dip, all three solutions are considered to be in agreement - they define an open, through-going continuous upper fracture zone from one end of the site to the other with an approximate N-S strike and an average essentially subhorizontal eastward dip of 1.4°. Clearly, three groups of overlapping solutions that yield nearly identical orientations support the explanation and existence of the subsurface feature. In addition, the solutions provide continuity for identifying the lateral extent of the fractures below the site.

Borings MR-102, MR-111, and MR-113 show similar traits as those above in that they indicate a marked decrease of REC % and RQD % in lower core runs below a reach of competent rock. Using these data, three-point problem solution #4 shows a secondary deeper (lower) open fracture oriented N52°E and dipping 5°SE (Figure 25). The lower fracture is not as wide (0.2' to 1.8' wide) as the upper fracture and occurs 10' to 14' deeper than the upper fracture with slightly steeper dip.

Thus, the three-point solutions have identified two horizons of open aperture fractures that descend across and below the site and dip gently eastward within the marble rock mass. They are hitherto unknown but important players in the subsurface hydrologic plumbing system that underlies the site as explained below.

GEOLOGY OF THE INWOOD MARBLE

Another pertinent aspect of the subsurface geology lies in the rock type variations that constitute the Inwood Marble Formation of NYC. The project site is covered by roughly 100' of overburden and then underlain by the venerable Inwood Marble Formation, originally named by Merrill et al. (1902). Formed from metamorphosed lower Paleozoic (~500 million year old)

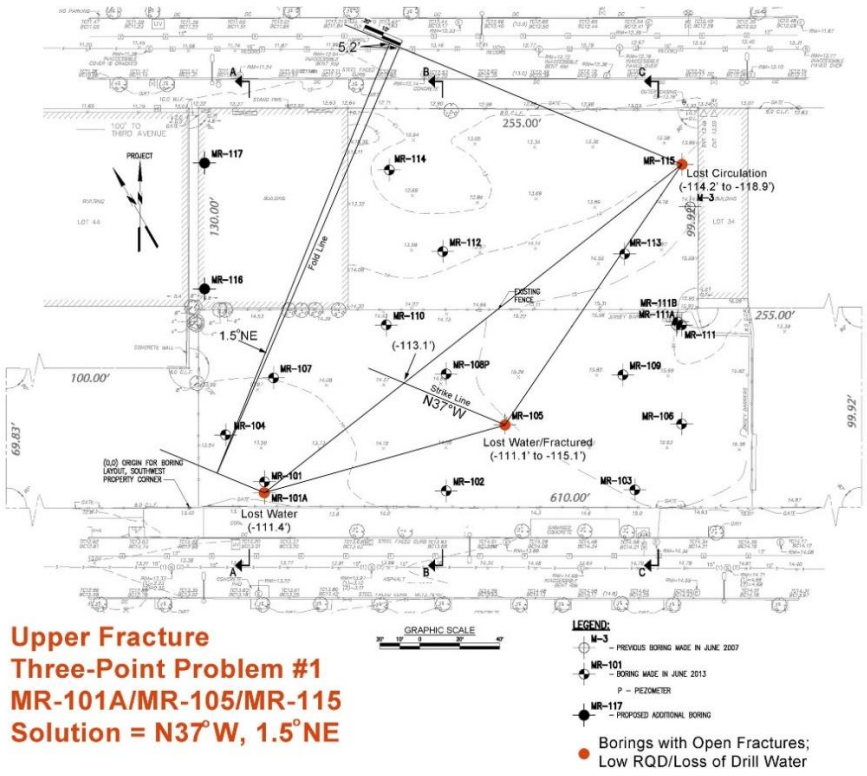

Figure 22 – Solution #1 for upper fracture. (Borings MR-101A, MR-105, and MR-115.)

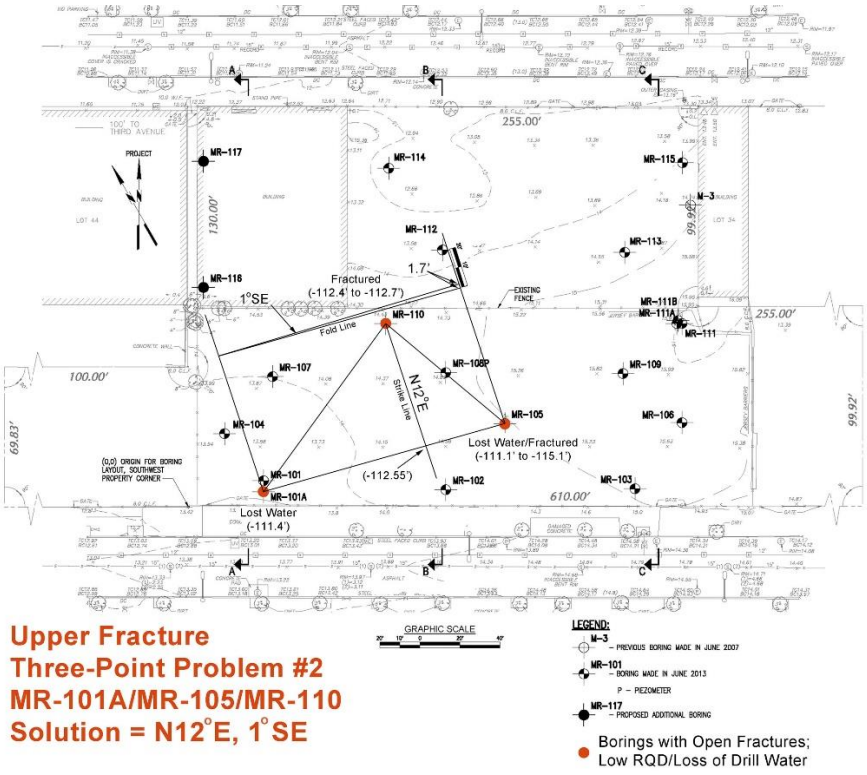

Figure 23 – Solution #2 for upper fracture. (Borings MR-101A, MR-105, and MR-110.)

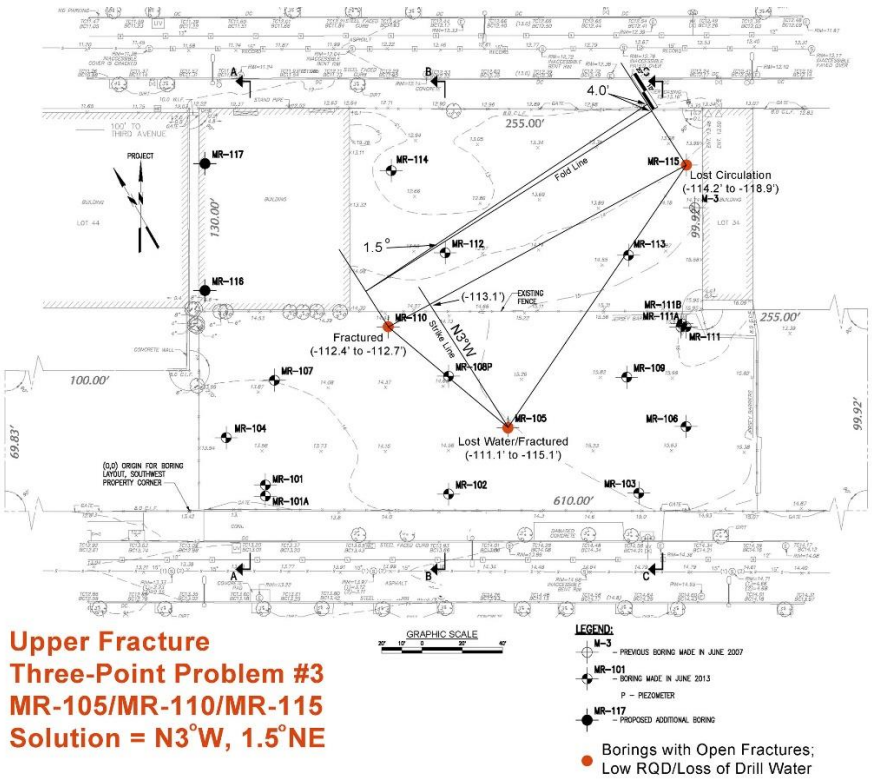

Figure 24 –Solution #3 for upper fracture. (Borings MR-105, MR-110, and MR-115.)

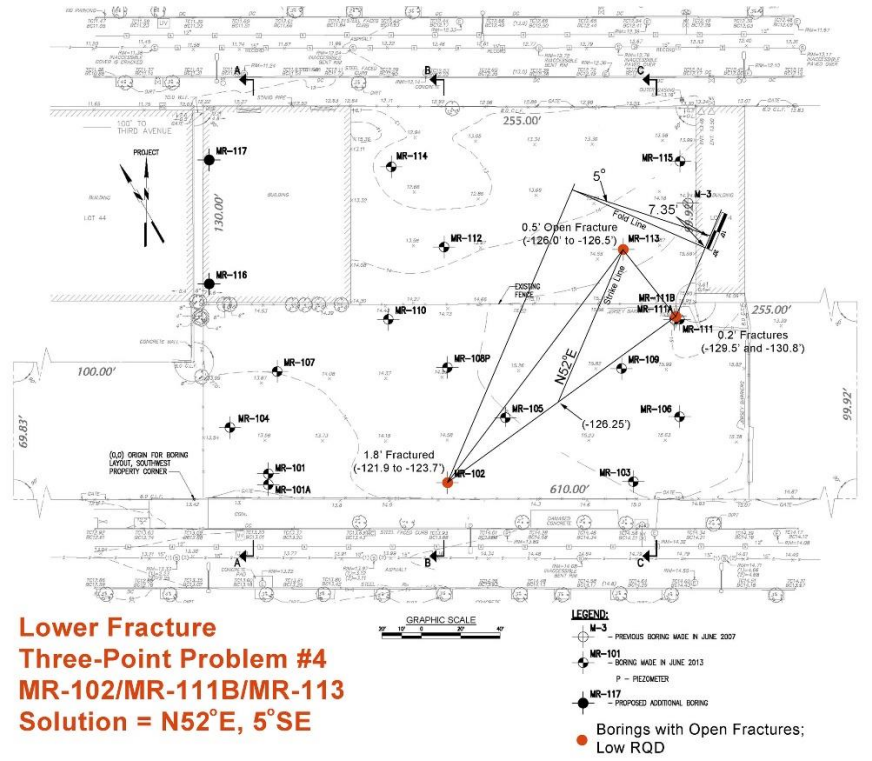

Figure 25 – Solution #4 for lower fracture. (Borings MR-102, MR-111B, and MR-113.)

former shallow water marine carbonate and clastic sediment, the Inwood Marble Formation now consists of well-layered, typically massive dolomitic and subordinate calcite marble. Constituting a folded layer over 700' thick in NYC, it underlies the Inwood section of northern Manhattan (type locality), the Harlem lowland NE of Central Park (this project site), occurs as thin belts in the East River channel, the subsurface of southeastern Manhattan and also crops out in the Bronx and Westchester County (Merguerian, Merguerian and Cherukupalli 2011).

But the devil they say, is in the details. By contrast to the **dolomitic** marble that constitutes the bulk of the Inwood Marble Formation in NYC a coarse-textured **calcite** marble is found near the top of the formation where it is interlayered with the overlying Walloomsac member of the Manhattan Schist (Merguerian 2008a, b). The same sub-unit was also found to underlie this site, based on rock samples collected during rock socket drilling and mucking operations. This unit, because it is a very coarse-textured pure calcite marble (+/- diopside and phlogopitic mica) rather than the typical dolomitic marble of the Inwood, it is susceptible to dissolution and disintegration along crystal boundaries and internal fractures by cold groundwater over time. Calcite ($CaCO_3$) is simply more soluble than dolomite ($Ca+Mg\ (CO_3)$) in cold fresh water. As such, this distinctive marble sub-unit unit is particularly prone to disintegration and weathering issues which can result in significant subsurface water transmissivity.

We have seen the coarse-textured white calcite marble sub-unit at the top of the Inwood Marble Formation at the top of rock at a project adjacent to the site and elsewhere in NYC (Isham Park, Inwood Park, and at a utility tunnel and associated large-diameter shaft site in the Bronx). What is more, our February 2017 examination of the drill core and acid testing of all of the core runs showed that the upper run (1C) of many of the borings (10 out of 17) were indeed exposing calcite marble at the top of the runs or in cored boulders resting presumably above the top of rock (MR-102, -103, -104, -106, -109, -110, -111B, -112, -114, and -115). The hint of the gentle inclination of the compositional layering (bedding) in this area allows for the interpretation that much of the "white marble" described in the logs at or near the top of rock is the same white calcite marble which can harbor open-aperture fractures and provide conduits for water (+/- sediment) transmission. The fact that calcite marble did not **always** result in difficulties indicates that the calcite marble is **not always** prone to disintegration. As we found in 2009 at a drill and blast large-diameter deep shaft site in the Bronx with similar overburden depth, calcite marble can be disintegrated and become water-bearing where it is cut by natural structural fractures in the rock mass that allowed groundwater interaction with the calcite marble to crumble and dissolve over time.

UNANTICIPATED GROUND CONDITIONS

The top of rock in NYC is hydrologically active, especially when overlain by over 100' of water-saturated unconsolidated regolith. Research performed by the U.S. Geological Survey in cooperation with the NYC DEP has shown that groundwater recharge in Manhattan takes place via percolation of meteoric water into NYC parks, especially Central Park (Stumm et al. 2001a, 2001b, 2004 and 2007) and is distributed radially away from the exposed bedrock knolls of central Manhattan outward. From there it permeates the soil (regolith) and also flows along the top of rock and into any existing bedrock conduits. Transmissive bedrock flow is often

facilitated by low-angle to horizontal open aperture fractures found throughout the crystalline bedrock of NYC but especially in the soluble sub-units of the Inwood Marble Formation as discovered at the 2009 shaft site in the Bronx (Stumm et al. 2013). Based on an extensive and detailed study, a very similar water-transmissive fracture system was found at this shaft site.

Two very gently inclined fracture zones descend below the top of rock at the job site based on the four fault plane solutions presented above. Figure 26 shows a conservative visualization of the gently east-dipping subsurface fracture system footprint (truncated blue ellipsoid) and shows a rather remarkable spatial coincidence with borings whose logs reported water loss during drilling and logs indicating fractures below more competent rock. The extended blue arrows with blue question marks are a reminder that the fractures certainly extend for some distance along strike and dip and may extend well beyond the zones shown in blue.

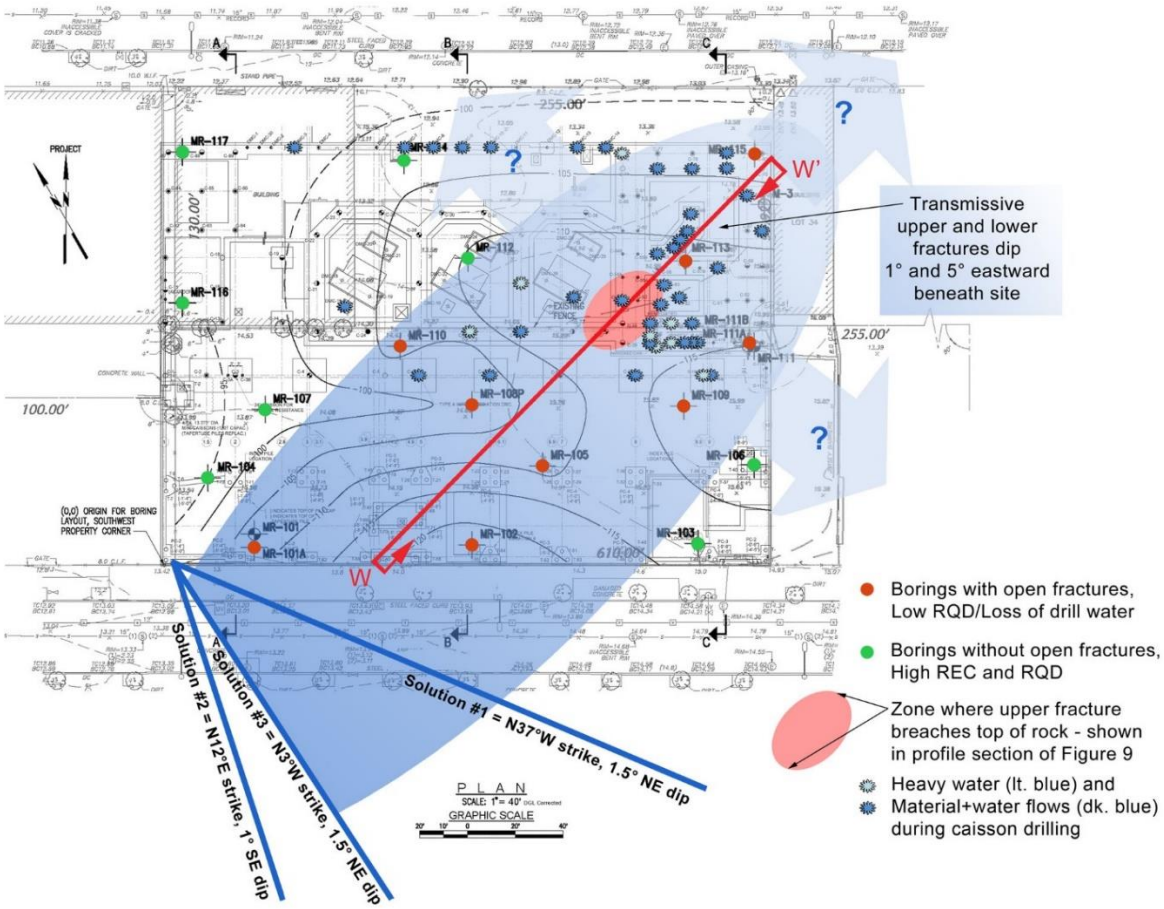

Figure 26 – Simplified plan map showing the three strike solution results of the three-point analyses presented in Figures 22 through 25 (dark blue lines) and the borings showing open fractures, low REC/RQD % and reported loss of drill water (red dots). Note the spatial coincidence of these borings with the projected footprint of the transmissive upper and lower fracture zones (eastward dipping blue ellipsoid) and their possible extensions down-dip and along strike (extended blue arrows). Also projected upward into plan view is the breached zone shown below in Figure 27 where the upper fracture zone is at or near the top of rock (pink ellipse).

Line of section W-W' depicts a vertical profile section of the subsurface condition that led to excessive water (Figure 27). The section was drawn using data provided by the geotechnical report, including the core logs, topographic map, depth to bedrock map and soil profiles and our three-point analyses. The upper fracture varies in width up to a potential maximum of 4.7' and slopes ~1° eastward across the site between -111' to -116' (elev.). The lower fracture slopes from -121' to -129' (elev.) southeasterly at 5° based on one fault plane solution (See Figure 25.) and strikes N52°E but shows similar traits. It appears to dip at 2° in the line of section (W-W' in Figure 27) since it would depict an apparent dip given the non-orthogonal angle between the strike and line of section. The strike for the upper fracture, as determined from the three-point problem solutions provided in Figures 22 through 24 ranges from N37°W to N12°E and thus averages roughly N-S as shown by the blue strike lines in Figure 26. Remember that strike varies greatly in sub-horizontal features. Clearly, the strike orientation of the lower fracture is not as well constrained given the solitary solution however we do not question its existence.

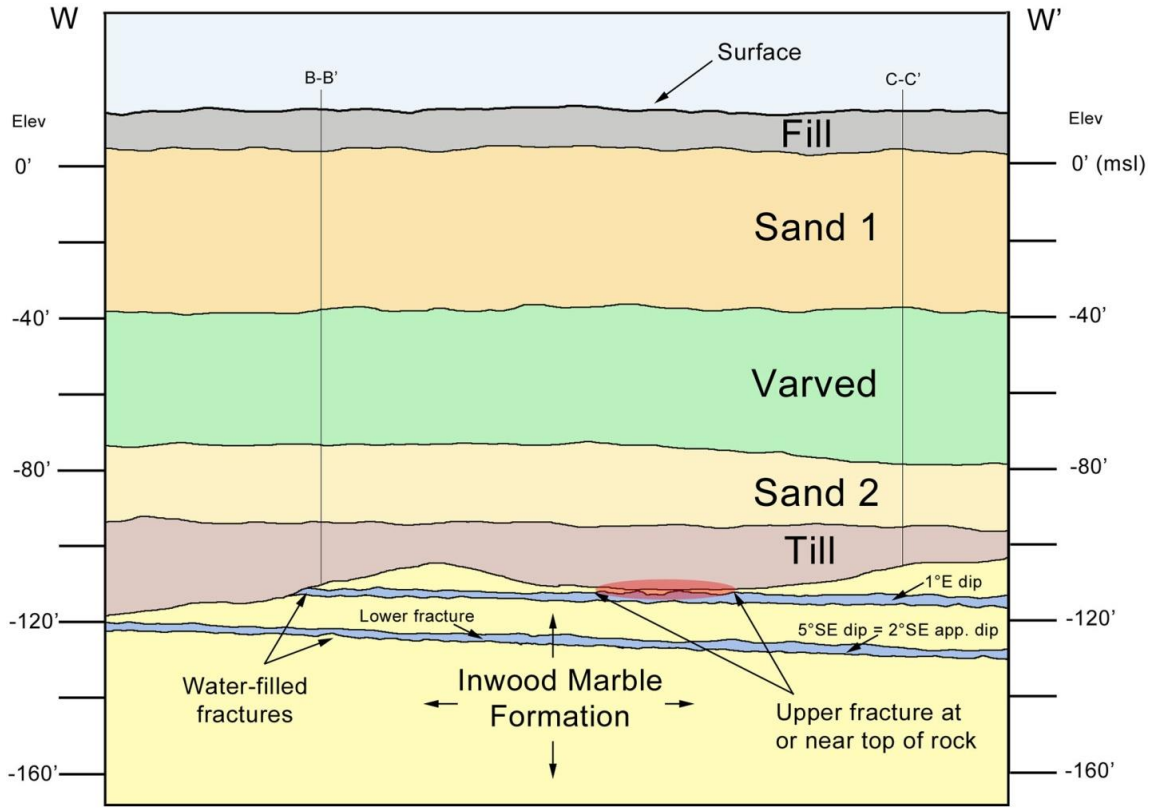

Figure 27 – Roughly west to east profile section (W-W') keyed to Figure 26 showing water-saturated overburden strata and Inwood Marble bedrock containing water-filled fracture zones (blue) detected beneath site using three-point problem solutions. Section is drawn roughly perpendicular to N-S strike of the upper bedrock fracture. Water-filled transmissive bedrock fractures from three-point solutions are based on our interpretation of data from boring logs and by using the top of rock contour map and geological sections provided by the geotechnical report for control. Note the unique bedrock to saturated overburden (water table ~+0.7' elev.) plumbing system provided by the open-aperture subsurface fracture zones that intercept the top of rock in a few places. (Drafted without vertical exaggeration.)

The profile section shows that the upper fracture zone intercepts the buried top of rock near borings MR-101A and MR-102. It intercepts and connects directly with the till unit of the regolith. Here, at the western corner of the site where top of rock slopes down, the lower fracture will also intercept the top of rock, but off-site.

Thus, **both fracture zones** intercept the top of rock and connect to water-saturated regolith toward the west and as such provides conduits for significant lateral flow of groundwater and sediment within the bedrock. Based on the data near MR-111B and MR-113, the upper fracture zone is at or near the fractured top of rock as shown diagrammatically by the pink elliptical zone in both map and profile section. (See Figures 26 and 27.) This hydrologic connection, even without any steep fractures, creates a unique plumbing system below the site with multiple direct connections between open water-bearing fractures from 0.2' to 4.7' in width and the permeable water-saturated regolith (water table ~+0.7' elev.).

A comparison of Figures 19, 20 and 26 shows very clearly the remarkable spatial correlation between the forty-four (44) caissons where drilling reports indicated deep water-related drilling issues (blue stars in Figure 19), borings with open fractures and/or low REC %/RQD % (red dots in Figure 20), the zone where the upper fracture is at or near the top of rock and the eastward dip and projected lateral flow extensions of the subsurface upper and lower fractures (pink ellipse, truncated blue ellipsoid and blue arrows in Figure 26). What is more, the fractures intercept the overburden and provide a unique plumbing system that apparently effected local hydrologic equilibrium when disturbed by drilling. Absent a detailed analysis as presented herein, the pre-bid information was simply inadequate to identify these deep geological features, their connectivity to the overburden, or to predict the drilling-related adverse effects.

TERRESTRIAL CAISSONS/PILES SUMMARY

This geotechnical investigation and associated maps and diagrams have shown that very gently inclined through-going upper and lower bedrock fractures provided open, laterally persistent subsurface conduits for fluids within the otherwise competent Inwood Marble rock mass. This has resulted in anomalous water and material transport particularly where the water-charged fractures were penetrated by construction drilling efforts. The provided three-point fracture plane solutions allow for visualization of the two very gently inclined open fractures that dip eastward from 1° to 5° at two different depths separated by about 10' of dominantly competent hard- to medium hard marble rock with high REC and RQD % values.

The differing site condition concept in lowest bid contracts allows for calculation of bids without adding increases for risk contingency. The purpose is to level the playing field and to make contractors whole when unforeseen ground conditions present themselves. We, using geological techniques, showed that the combined effect of open-aperture fissures in bedrock dipping beneath the site provided a unique plumbing system that allowed for hydrologic connectivity and localized communication between the drilled caisson sites, the water-saturated till (T) and confined lower sand layer (Sand 2) and the bedrock (R). This geological condition resulted in ground effects that impeded construction. As such, this can only be considered a valid DSC since no mention of this natural geological condition was described in the pre-bid documents.

No contractor would be able to perform such an analysis as presented above nor retain an expert to arrive at this result pre-bid nor would such an analysis be expected based on the geotechnical information provided. (Compare Figures 19 and 27.) Our opinion at the time of this consult was that if a geological expert with intimate knowledge of the as-built experience and the regional geology were able to evaluate the pre-bid core and core logs he or she may have been able to provide a "look-back explanation" to explain the ground conditions (as we have done in this segment) but no contractor could have predicted or anticipated the true ground condition pre-bid nor its effects on construction based on the supplied geotechnical information - a hallmark of a valid DSC claim.

REFERENCES

Publications by the authors can be found at www.Dukelabs.com under the Publications tab.

Bennington, J Bret, and Merguerian, Charles, 2007, Geology of New York and New Jersey: Physical Geology Textbook Supplement, 24 p.: in Essentials of Geology with Geology of New York and New Jersey: Thomson Brooks/Cole, 510 p.

Brock, Pamela Chase; Brock, Patrick W. G.; and Merguerian, Charles, 2001, The Queens Tunnel Complex: a newly discovered granulite facies Fordham orthogneiss complex that dominates the subsurface of western Queens: p. 1-8 *in* Hanson, G. N., *chm*., Eighth Annual Conference on Geology of Long Island and Metropolitan New York, 21 April 2001, State University of New York at Stony Brook, NY, Long Island Geologists Program with Abstracts, 128 p.

Donn, W. L., and Shimer, J. A., 1958, Graphical methods in structural geology: Appleton-Century-Crofts, Inc., NY, 180 p.

Merguerian, Charles, 1994, Stratigraphy, structural geology, and ductile- and brittle faults of the New York City area, p. 49-56 *in* Hanson, G. N., *chm*., Geology of Long Island and metropolitan New York, 23 April 1994, State University of New York at Stony Brook, NY, Long Island Geologists Program with Abstracts, 165 p.

Merguerian, Charles, 2001, Young rhyodacite dikes found in the Queens Tunnel, beneath Woodside, Queens: p. 9-19 *in* Hanson, G. N., *chm*., Eighth Annual Conference on Geology of Long Island and metropolitan New York, 21 April 2001, State University of New York at Stony Brook, NY, Long Island Geologists Program with Abstracts, 128 p.

Merguerian, Charles, 2002, Brittle Faults of the Queens Tunnel Complex, NYC Water Tunnel #3: p. 63-73 *in* Hanson, G. N., *chm*., Ninth Annual Conference on Geology of Long Island and metropolitan New York, 20 April 2002, State University of New York at Stony Brook, NY, Long Island Geologists Program with Abstracts, 116 p.

Merguerian, Charles, 2005a, Geological controls on effective hard-rock TBM tunneling in crystalline terrains: *in* 84th Annual Meeting, 9-13 January 2005, Compendium of Papers CD-ROM, Transportation Research Board of the National Academies, 11 p.

Merguerian, Charles, 2005b, Lithologic and structural constraints on TBM tunneling in New York City (NYC), p. 704-724 *in* Hutton, John D. and Rogstad, W.D., *eds.*, Rapid Excavation and Tunneling Conference, 2005 Proceedings Society of Mining, Metallurgy, and Exploration, 1371 p.

Merguerian, Charles, 2008a, Evaluating geological controls on hard rock excavation, New York City, NY: *in* Proceedings, Manhattan On the Rocks, American Society of Civil Engineers, Metropolitan Section, 08 May 2008, 31 p.

Merguerian, Charles, 2008b, Geological controls on means and methods of hard rock excavation, New York City, NY: p. 79-109 *in* Gorring, M. L., ed., Environmental and Engineering Geology of Northeastern New Jersey, Geological Society of New Jersey, XXV Annual Conference Proceedings, 17 October 2008, 111 p.

Merguerian, Charles, 2015, Review of New York City bedrock with a focus on brittle structures; *p. 17-67 in Herman, G. C. and Macaoay Ferguson, S., eds.*, Geological Association of New Jersey Guidebook, Neotectonics of the New York Recess, 32nd Annual Conference and Field Trip, Lafayette College, Easton, PA, 214 p.

Merguerian, Charles; and Merguerian, J. Mickey, 2012, Structural geology and metamorphism of the Inwood Marble, NYC, NY: Geological Society of America Abstract # 199974, Abstracts with Programs, v. 44, no. 2, p. 73.

Merguerian, Charles; Merguerian, J. Mickey; and Cherukupalli, Nehru, E., 2011, Stratigraphy, structural geology and metamorphism of the Inwood Marble Formation, northern Manhattan, NYC, NY: *in* Hanson, G. N., *chm*., Eighteenth Annual Conference on Geology of Long Island and Metropolitan New York, 09 April 2011, State University of New York at Stony Brook, NY, Long Island Geologists Program with Abstracts, 19 p.

Merguerian, Charles; and Ozdemir, Levent, 2003, Rock Mass Properties and Hard Rock TBM Penetration Rate Investigations, Queens Tunnel Complex, NYC Water Tunnel #3, Stage 2: p. 1019-1036 *in* Robinson, R.A. and Marquardt, J.M., *eds.*, Rapid Excavation and Tunneling Conference, 2003 Proceedings Society of Mining, Metallurgy, and Exploration, 1334 p.

Merrill, F. J. H., and others, 1902, Metamorphic crystalline rocks of the New York City quadrangle, *in* Merrill, F. J. H.; Darton, N. H.; Hollick, Arthur; Salisbury, R. D.; Dodge, R. E.; Willis, Bailey; and Pressey, H. A., Description of the New York City district: United States Geological Survey Geologic Atlas of the United States, New York City Folio, No. 83, 19 p. (Includes colored geologic map on a scale of 1:62,500).

Spear, F. S. (1993) Metamorphic Phase Equilibria and Pressure-Temperature-Time Paths: Mineralogical Society of America Monograph, Mineralogical Society of America, Washington, D. C., 799 p.

Stumm, Frederick, Chu, Anthony, Lange, Andrew D., Paillet, Frederick L., Williams, John H., and Lane, John W., Jr., 2001a, Use of advanced borehole geophysical techniques to delineate fractured-rock ground-water flow and fractures along water-tunnel facilities in Northern Queens County, New York U.S. Geological Survey Water-Resources Investigations Report 00-4276, 12 p.

Stumm, Frederick, Chu, Anthony, Lange, Andrew D., 2001b, Use of advanced borehole geophysical and techniques to delineate fractured-rock ground-water flow, faults, foliation, and fractures along the western part of Manhattan, New York: U.S. Geological Survey Open-file Report 2001-196, 46 p.

Stumm, Frederick, Chu, Anthony, and Monti, Jack, Jr., 2004, Delineation of faults, fractures, foliation, and ground-water-flow zones in fractured-rock, on the southern part of Manhattan, New York, through use of advanced borehole-geophysical techniques, U.S. Geological Survey Open-File Report 2004-1232, 212 p.

Stumm, F., Chu, A., Joesten, P.K., and Lane, J.W., 2007, Geohydrologic assessment of fractured crystalline bedrock on the southern part of Manhattan, New York, through use of advanced borehole geophysical methods: Journal of Geophysics and Engineering, Vol. 4, No. 3, 8 p.

Stumm, Frederick; Chu, Anthony; Joesten, P. K., Noll, M. L., and Como, Michael, 2013, Delineation of fractures, foliation, and groundwater flow zones of the bedrock at the Harlem River tunnel in northern New York County, New York: *in* Hanson, G. N., *chm*., Twentieth Annual Conference on Geology of Long Island and Metropolitan New York, 13 April 2013, State University of New York at Stony Brook, NY, Long Island Geologists Program with Abstracts, 12 p.